RN-24, May 1965

AD617934

61-p
as
3.00
0.75

ELECTRO-OPTICAL SYSTEMS, INC.
RESEARCH NOTES

TURBULENT MIXING IN THE BASE FLOW REGION

Hartley H. King and M. Richard Denison

ARCHIVE COPY

Handed down from the Middle Ages, these mystic symbols were representative of the four elements in nature: ⚟ air, ▽ water, ⚶ earth, and △ fire. Modern science has since identified these four elements with the four states in which matter appears in the universe: gas, liquid, solid, and plasma. Understanding the properties of matter in these four forms is the basis of modern and future technology.

54

EOS Research Note No. 24, May 1965

TURBULENT MIXING IN THE BASE FLOW REGION

Hartley H. King and M. Richard Denison

ELECTRO-OPTICAL SYSTEMS, INC. Pasadena, California

A Subsidiary of Xerox Corporation

-4

SUMMARY

An exploratory study is made in connection with the problem of predicting properties of the turbulent base flow region of a body at hypersonic speeds. An attempt is made to calculate the gross features of the base flow using a non-similar mixing model including the Chapman-Korst recompression condition. The expression for the eddy viscosity is based on a model which allows the turbulent equations to be transformed into incompressible laminar form. The empirical factor in the eddy viscosity expression is evaluated from data obtained from the near field (in the linear growth region) of jets exhausting into a quiescent region. The same expression for the eddy viscosity is then used in an attempt to estimate the growth of non-similar turbulent mixing layer using both turbulent and laminar initial profiles.

The correlation of turbulent jet mixing data for speeds up to Mach 3 shows that the eddy viscosity is a very strong function of Mach number (or of density ratio across the jet, since the data are for adiabatic flow). If the eddy viscosity dependence on density ratio persists for density ratios typical of re-entry conditions, then it is found that at these conditions the growth rate of the turbulent shear layer is orders of magnitude slower approaching the rate of growth of the laminar mixing layer under the same conditions. This is in marked contrast to the situation at low supersonic speeds, where the turbulent mixing layer dividing streamline velocity approaches the similar value well before recompression occurs. If this speculation is correct, then the stagnation enthalpy at recompression in the hypersonic turbulent base flow should be well below the total enthalpy value, since the enthalpy build-up on the dividing streamline will be similarly suppressed.

This research is a part of PROJECT DEFENDER, sponsored by the Advanced Research Projects Agency, Department of Defense, under ARPA Order No. 254-62, monitored by Air Force Ballistic Systems Division under Contract No. AF 04(694)-570.

TABLE OF CONTENTS

		Page
1.	INTRODUCTION	1
2.	EDDY VISCOSITY	2
3.	CONSERVATION EQUATIONS	5
4.	SIMILAR SOLUTION	9
5.	CORRELATION WITH EXPERIMENT	11
6.	NON-SIMILAR SOLUTION	15
7.	LAMINAR INITIAL CONDITIONS	17
8.	TRANSFORMATION INVERSION - LAMINAR BODY	18
9.	TURBULENT INITIAL CONDITIONS	20
10.	TRANSFORMATION INVERSION - TURBULENT BODY	27
11.	NUMERICAL SHEAR LAYER CALCULATIONS	28
12.	BASE FLOW OF CONE OR WEDGE	30
13.	RESULTS FOR 10° CONE	33
14.	CONCLUDING REMARKS	36
	REFERENCES	37
	APPENDIX A	40
	APPENDIX B	41

ILLUSTRATIONS

1. Mixing Layer Regions 44
2. Geometry of the Jet Mixing Experiment 44
3. Experimental Dividing Streamline Velocity Calculated from Mass Balance 44
4. Correlation of Profile Data 45
5. Correlation to Determine the Eddy Viscosity Factor k 45
6. Equivalent Skin Friction Coefficient $\overline{C}_f$ for Cones and Wedges, $H_w/H_e = 0$ 46
7. Equivalent Skin Friction Coefficient $\overline{C}_f$ for Cones and Wedges, $H_w/H_e = 1$ 46
8. Effect of Wall Enthalpy Ratio on $\overline{C}_f$ for $\tilde{R} = 10^7$ 46
9. Turbulent Initial Mixing Layer Profile 46
10. Development of the Velocity Gradient Profiles with Streamwise Distance 47
11. Development of the Enthalpy Function W Profiles with Streamwise Distance 48
12. Velocity on the Dividing Streamline 49
13. Enthalpy Function W on the Dividing Streamline 49
14. Relation Between x* and S* 50
15. Shear Layer Momentum Thickness Integral 50
16. Base Flow Model 51
17. Dividing Streamline Velocity Before Recompression 51
18. Recirculating Region Enthalpy 51
19. Effect of Mach Number on Centerline Static Enthalpy After Recompression 52
20. Effect of Reynolds Number on Centerline Static Enthalpy After Recompression 52
21. Effect of Mach Number on Base Pressure 52
22. Effect of Reynolds Number on Base Pressure 52

ACKNOWLEDGEMENT

The authors wish to express their appreciation to Dr. Eric Baum for providing the computer program for calculation of the non-similar mixing layer profiles of this report.

1. INTRODUCTION

Predictions of observables in the wakes of slender re-entry vehicles have been found to depend crucially on the flow properties assumed at the neck region. For example, predicted electron densities and radar cross-sections of wakes may vary by orders of magnitude, depending on the assumed value of the centerline neck enthalpy ratio h/H_e.[1] Since properties at the wake neck are determined by the flow processes in the body boundary layer and base flow mixing regions, it is clear that accurate methods for flow calculations in these regions must be developed.

The primary objective of the present paper is to devise a procedure for calculating the gross properties of the hypersonic turbulent base flow (e.g. base pressure, neck enthalpy, etc.). The problem is approached from the point of view of the generalized Chapman-Korst base flow model, as was done in the laminar case.[2,3] For laminar flow this model is thought to be reasonable for moderate supersonic Mach numbers, but is probably not adequate for re-entry conditions. Recently, Reeves and Lees,[4] Webb, Golik and Lees,[5] and others have attempted to devise base flow models more applicable to re-entry conditions. These methods are not yet well established and still may not contain essential features even for the laminar case. For turbulent flow the difficulty is compounded by uncertainties related to the "eddy" transport coefficients, so it seems more reasonable to use the simpler Chapman-Korst model at the present time. If this procedure is adopted, then what remains is to develop a reasonable empirical model for the eddy coefficients. A major part of the present paper is devoted to this task.

Having developed appropriate expressions for the eddy coefficients, one can then solve the non-similar mixing layer equations, and thereby determine how rapidly the profiles change from the initial distributions on the body at separation to the fully-developed profiles far downstream

from separation. For the base flow this rate of change or build-up of the profiles may be of crucial importance if recompression occurs before the asymptotic or fully developed condition is approached. This is the situation occurring in laminar case, [2,3] and could also occur in the turbulent case.

The present report contains three separate parts. The first shows that experimental turbulent mixing data can be correlated by an eddy viscosity model based on the assumption that $\rho\varepsilon$ = function of x only. Thus the effect of compressability is taken into account in the same manner as with laminar flow; the effect of turbulence thereby being placed in the streamwise variable transformation. The second part of the report deals with the solution of the non-similar mixing layer problem, assuming that the previously developed expression for the eddy viscosity remains valid even near the separation point. The third portion of the report utilizes the results of the non-similar mixing layer analysis and the Chapman-Korst base flow model to predict the base flow properties of a highly cooled slender cone under re-entry conditions.

As might be expected, the results of this report depend crucially on the expression developed for the eddy viscosity. Unfortunately, the available data cover a very limited Mach number range and are for essentially adiabatic flow, so that a considerable extrapolation is involved in applying the model to the re-entry case. Thus the final base flow results presented must be considered tentative and subject to revision when new turbulent mixing data become available.

2. EDDY VISCOSITY

A fundamental assumption of this report is that the compressible mixing layer flow can be transformed to an equivalent incompressible flow. The transformation is of the type used by Mager,[6] Burggraf[7] Ting and Libby[8] and others, in which the stream function and shear stress over a mass element are assumed invariant. In the incompressible plane the eddy viscosity is assumed to be given by Prandtl's expression,[9] and is proportional to the width of the mixing zone and the velocity difference across the layer. Ferri[10] recently has argued that when generalized to compressible flow, Prandtl's expression should be proportional to the tangential mass flux difference instead of the velocity difference. For mixing layers with negligible flow on the inside both expressions are identical. A more serious defect is that the eddy viscosity is assumed to suddenly change from a form suitable to the body boundary layer to that characteristic of the mixing layer after the shoulder expansion.

With these assumptions the resulting compressible eddy viscosity is the following:

$$\epsilon = k \frac{\rho_e^2}{\rho} u_e b \tag{1}$$

In Eq. (1) k is a dimensionless proportionality factor to be determined by correlating the theory with experimental data and is at most a function of the external flow conditions. The quantity b is a suitably chosen width of the mixing layer and ρ_e is a reference density used to give ϵ the dimensions of viscosity. As pointed out by Ting and Libby, Eq. (1) implies that ϵ is variable across the mixing zone because of the density variation, whereas in the incompressible case it is constant. For the mixing layer the width is assumed to be:

$$b = \theta = \int_{-\infty}^{\infty} u^*(1-u^*) \frac{\rho}{\rho_e} dy \tag{2a}$$

so that ϵ is proportional to the momentum thickness of the mixing layer. We could also try for the width

$$b = \int_{y_1}^{y_2} \frac{\rho}{\rho_e} dy \tag{2b}$$

where (by convention) y_1 and y_2 are respectively the values of y where $u^{*2} = 0.1$ and 0.9. It turns out that Eqs. (2a) and (2b) produce essentially the same final results for a mixing layer of negligible initial thickness. For the more general problem however, Eq. (2a) seems more reasonable than (2b). The only justification for these assumptions for b at present is that they simplify the analysis somewhat by uncoupling the energy terms from the momentum equation. As with all turbulent theories of this type, further justification for the selection of the expression for ϵ must come by comparing the results of the analysis with experimental data.

3. CONSERVATION EQUATIONS

The boundary layer equations involving the mean flow variables are assumed to be appropriate for the description of the constant pressure mixing region (Fig. 1), provided the exchange coefficients are replaced by their empirical turbulent counterparts. In spite of the well recognized fact that energy, species, and momentum transport may occur by different mechanisms in turbulent flow, we simplify matters by assuming that $Pr_t = Le_t = 1$. Then only the eddy viscosity is used explicitly. This rough model later may be refined the results prove promising. The equations are:

$$(\rho u r_o^{\,j})_x + (\rho v r_o^{\,j})_y = 0 \tag{3a}$$

$$\rho u u_x + \rho v u_y = (\epsilon u_y)_y \tag{3b}$$

$$\rho u H_x + \rho v H_y = (\epsilon H_y)_y \tag{3c}$$

where $r_o = r_o(x)$ is the mean radius of the thin mixing layer in the axisymmetric case. The boundary conditions are (Fig. 1):

$y = -\infty$:	$u = 0,\ H = H_c$ (constant)	(4a)
$y = \infty$:	$u = u_e,\ H = H_e$	(4b)
$y = 0$:	$v = 0$ (dividing streamline)	(4c)
$x = 0,\ y \geq 0$:	u = given initial velocity profile	(4d)
	$H = H_e - (H_e - H_w)\ (1-u^*)$ (Crocco Integral)	(4e)

Since we wish to consider cases where $H_c \neq H_w$, the Crocco integral is not applicable in the mixing region, although it is assumed to apply initially (at the body base, x = 0). Thus, as in the laminar case,[11] introduce an auxiliary enthalpy function W which is related to H as follows:

$$H = H_e - (H_e - H_c)(1 - u^*) - (H_c - H_w)\, W \tag{5}$$

Then the W equation is

$$\rho u W_x + \rho v W_y = (\epsilon W_y)_y \tag{6a}$$

$$W(-\infty) = W(\infty) = 0 \tag{6b}$$

$$W(x = 0) = 1 - u^* \tag{6c}$$

This allows the energy equation to be solved without explicit knowledge of the core enthalpy H_c. With W available the enthalpy profile may be calculated from Eq. (5) after H_c is specified.

In order to transform the equations to incompressible form the usual transformation of the y coordinate is introduced. Let

$$Y = \rho_e u_e r_o^{\,j} \int_0 \frac{\rho}{\rho_e}\, dy \tag{7a}$$

and define

$$u^* = u/u_e \tag{7b}$$

$$F = \frac{\partial u^*}{\partial Y} \tag{7c}$$

Then

$$\rho\epsilon = k\, \rho_e r_o^{-j} \Phi \tag{8a}$$

where

$$\Phi(x) = \int_0^1 \frac{u^*\,(1-u^*)\, du^*}{F} \tag{8b}$$

Introduction of relations (7) and (8) in the conservation equations (3) and further transformation to Crocco coordinates yields

$$u^* \frac{\partial F}{\partial x} = (\rho_e u_e r_o^{\,j} k\ \Phi)\ F^2 \frac{\partial^2 F}{\partial u^{*2}} \tag{9}$$

and a similar expression for W. The factor in parentheses on the right hand side depends on x only, although Φ depends upon the solution. Therefore Eq. (9) can be put in the form of the laminar momentum equation if we define

$$dS^* = F_w^{\,2}\ (\rho_e u_e r_o^{\,j} k\ \Phi)\ dx \tag{10a}$$

$$F^* = F/F_w \tag{10b}$$

where F_w is the value of F on the body before separation.

Then the conservation equations become

$$u^* \frac{\partial F^*}{\partial S^*} = F^{*2} \frac{\partial^2 F^*}{\partial u^{*2}} \tag{11a}$$

$$u^* \frac{\partial W}{\partial S^*} = F^{*2} \frac{\partial^2 W}{\partial u^{*2}} \tag{11b}$$

These equations are in a form identical to the laminar equations and also have the same boundary conditions as in the laminar case. The differences are in the inversion of S^* back to physical space and in the initial conditions. If the body boundary layer is turbulent, initial conditions for the mixing layer must take this into account. On the other hand it is conceivable that the body boundary layer might be laminar with transition occurring at the shoulder. In this case the initial profile will also correspond to the laminar case.

For a laminar body boundary layer the initial and boundary conditions are:

$$S^* = 0: \quad F^*(0,u^*) = f''_B(\eta_B)/f''_B(0) \tag{12a}$$

$$W(0,u^*) = 1-u^* \tag{12b}$$

$$u^* = 0: \quad F^*(S^*,0) = W(S^*,0) = 0 \tag{12c}$$

$$u^* = 1: \quad F^*(S^*,1) = W(S^*,1) = 0 \tag{12d}$$

where f''_B is obtained from the Blasius solution (see Section 7). These equations have been previously solved and the solution tabulated.[11]

The problems remaining, then, are the inversion of the turbulent flow transformation S^* back to physical space and establishment of initial conditions for turbulent flow on the body.

4. SIMILAR SOLUTION

A first step in inverting the turbulent solution is to obtain the parameter k from experiments. For this purpose we investigate similar solutions which can then be compared with experimental data. It is known from the laminar case that at large values of S^* the effect of the initial structure of the shear layer will disappear and the solution will asymptotically approach the similar solution of Chapman.[10] Since the turbulent problem has been made mathematically equivalent to the laminar case with the exception of initial conditions, the asymptotic solutions must be identical.

In order to obtain the Blasius equation instead of its counterpart in Crocco coordinates we introduce the normal distance parameter

$$\eta = \frac{YF_w}{(2S^*)^{1/2}} \tag{13a}$$

Then the velocity is assumed to be a function of η only

$$u^* = f'(\eta) \tag{13b}$$

When Eqs. (13a) and (13b) are introduced in the conservation equations the familiar results are obtained.

$$f_{\eta\eta\eta} + ff_{\eta\eta} = 0 \tag{14a}$$

$$W_{\eta\eta} + fW_{\eta} = 0 \tag{14b}$$

The boundary conditions are $f_\eta(-\infty) = 0$, $f_\eta(\infty) = 1$, $W(-\infty) = W(\infty) = 0$, and $f(0) = 0$. The last condition follows from the specification that

$\eta = 0$ corresponds to the dividing streamline. Clearly the solution for W is $W \equiv 0$, which of course implies the usual Crocco integral relation for the total enthalpy from Eq. (5). The solution for f may be obtained from tabulations by Chapman[12] and Christian[13].

The momentum thickness function for the similar solution is given by

$$\Phi = \frac{(2S^*)^{1/2}}{F_w} c \tag{15a}$$

where

$$c = \int_{-\infty}^{\infty} f'(1-f')\, d\eta = .8756 \tag{15b}$$

Use of Eq. (15) in Eq. (10) and integration yields:

$$(2S^*)^{1/2} = k\, c\, F_w \int_0^x \rho_e u_e r_o^{\,j} dx \tag{16a}$$

Hence

$$\eta = \frac{Y}{\xi} \tag{16b}$$

where

$$\xi = k\, c \int_0^x \rho_e u_e r_o^{\,j} dx = (2S^*)^{1/2}/F_w \tag{16c}$$

It can be seen from Eqs. (16b) and (16c) as well as the definition of Y, Eq. (7a), that the similarity parameter η becomes proportional to y/x for a two dimensional incompressible flow, which is a well known behavior.

5. CORRELATION WITH EXPERIMENT

The primary source of correlation is obtained from experiments dealing with the turbulent flow of jets exhausting into a quiescent region (Fig. 2). The region most applicable to the problem of the base flow is the mixing zone between the jet exit and about five diameters downstream. This type of flow is "inside-out" compared with the base flow problem, since the high velocity flow is inside the mixing region rather than outside. This hopefully will not make any difference, so that if the jet experimental data can be correlated with the theory, then the theoretical results can be applied directly to the base flow problem.

The primary source of data for the eddy viscosity correlation of this report is the work of Maydew and Reed,[14] who measured velocity profiles in the near mixing region of turbulent jets exhausting into the atmosphere. The nozzle exit diameter of these experiments was 3", and profile data were obtained for exit Mach numbers .7, .85, .95, 1.49, and 1.96 at five axial stations in the range $1.5'' \leq x \leq 11.5''$. Leipmann and Laufer[15] also give data for $M \approx .05$, while some earlier data of possible applicability to the present problem are referred to by Maydew and Reed.

One result which can be compared with the theory is the velocity on the dividing streamline. According to the solution of Eq. (14a) this value should be $u^* = .587$ if the flow is sufficiently downstream of separation for similarity to hold. In order to check this result, the jet mixing profiles of Maydew and Reed[14] were integrated outward from the axis of the jet until the mass in the profile was equal to the mass flowing throu[illegible] the jet. In these calculations the Crocco integral relation was used to calculate the density variation, and the entrance mass was calculated from the measured stagnation temperature and pressure, assuming an isentropic one-dimensional expansion. Further details regarding this mass balance are given in the Appendix.

Fig. 3 shows the calculated results of the mass balance for the five exit Mach numbers of the experiments of Maydew and Reed. One sees that the calculated experimental dividing streamline velocity u^* is about 0.6 or perhaps a little higher. It is substantially independent of streamwise distance for $x/d \gtrsim 1$, indicating that the mixing region has probably reached similarity. It should be noted, however, that the accuracy of the integration procedure is very poor for stations close to the jet exit, since most of the mass flow inside the dividing streamline is in the potential core and not in the mixing profile (see Fig. 2). Under these conditions a small error in the mass flow calculation will produce a large error in the value of u^* on the dividing streamline. Further, the use of the Crocco integral for the density variation may be questioned. We therefore conclude from Fig. 3 that the dividing streamline velocity data agree with the present theory within the possible error of the measurements and integration procedure, but these data are probably too crude to constitute a critical test.

The second and more important portion of the data correlation concerns the fitting of the theoretical velocity profile to the data. This has traditionally been done by finding the best numerical value of the "spreading parameter" σ such that the velocity profile is represented by

$$u^* = g(\sigma \frac{y}{x}) \tag{17}$$

where g is a profile function specified beforehand. For example, the error function profile is frequently used, while Maydew and Reed find that the data correlate well with the results of Crane.[16] The numerical value of σ for "best fit" of course depends on the choice of profile. A certain arbitrariness also exists in the selection of the profile position from which y is measured, and this traditionally is taken as the location where $u^* = .5$ for the data.

We begin by noting that the present solution for compressible flow does not allow the physical velocity profile to be expressed in the form of Eq. (17). This of course is due to the manner in which the effect of compressibility is included in the transformation. To derive the form of the velocity profile in the physical coordinates, the Howarth integral in the expression for η must be inverted. This can be done by assuming perfect gas behavior (which is reasonable for the Maydew-Reed experiments) and using the Crocco integral relation. Thus for a perfect gas:

$$\frac{\rho_e}{\rho} = \frac{h}{h_e} = \frac{H_e}{h_e}\left[\frac{H_c}{H_e} + \left(1 - \frac{H_c}{H_e}\right)u^* - \left(1 - \frac{h_e}{H_e}\right)u^{*2}\right] \tag{18a}$$

$$\frac{H_e}{h_e} = 1 + \frac{\gamma-1}{2} M_e^{\ 2} \tag{18b}$$

Then if r_o is assumed to be constant, one finds that

$$\frac{y}{x} = kc\left(\frac{H_e}{h_e}\right)\left[\frac{H_c}{H_e}\eta + \left(1 - \frac{H_c}{H_e}\right)f - \left(1 - \frac{h_e}{H_e}\right)\int_o^\eta f_\eta^2 \, d\eta\right] \tag{19}$$

Since $u^* = f_\eta(\eta)$, it is clear that an expression for u^* of the form of Eq. (17) is not possible.

To compare with the velocity profile data of Maydew and Reed, Eq. (19) is multiplied by σ, where σ is now considered to be just a given scale factor for each set of profile data. Also in the above, for convenience y is measured from the position for $u^* = .587$, rather than $u^* = .5$, as done by Maydew and Reed.

It is assumed that $H_c/H_e = 1$, since this was assumed in the Maydew-Reed data reduction, even though $.93 < H_c/H_e < 1$ for their experiments.

Also $x = x_e + \Delta x$, where x_e is the experimental distance from the jet exit and Δx is an additional incremental distance to the "virtual origin" of the turbulent mixing layer as tabulated by Maydew and Reed.[14]

Fig. 4 shows the correlation of the Maydew-Reed data with the Chapman profile for the various experimental Mach numbers. The constant k was first obtained by finding the "best fit" of Eq. (19) with each set of profile data, using a "least squares" analysis. (Note that the momentum thickness factor c = .8756 from the Chapman solution.) The theoretical curves shown, however, are based on the final equation for the correlation constant, as described below. It is seen that the shapes of the profiles seem to correlate quite well. This is perhaps not too surprising, however, since many curves of this general shape seem to correlate in a reasonable manner if the adjustable constant is properly chosen.

It was hoped initially that the quantity k would not be a function of Mach number, but would be a universal constant. Instead it is found to vary quite strongly with Mach number for $.05 \leq M \leq 3$. It is reasonable to assume that this variation is related to the density ratio across the mixing region ρ_e/ρ_c. For a perfect gas this is equal to H_c/h_e, and if the flow is completely adiabatic, then $\rho_e/\rho_c = H_e/h_e = (1 + \frac{\gamma-1}{2} M_e^2)$. Figure 5 shows a log-log plot of k as a function of ρ_e/ρ_c, assuming adiabatic flow. Based only on the Maydew-Reed data, it is found that very nearly

$$k = b_1 \left(\frac{\rho_c}{\rho_e}\right)^{b_2} \qquad \begin{aligned} b_1 &= .0606 \\ b_2 &= 2.0 \end{aligned} \tag{20}$$

If the data of Leipmann and Laufer and tentative data of Zumwalt (see Appendix) had been included in the correlation, the constants in Eq. (20) would probably be changed slightly. Thus for the similar solution:

$$\rho\epsilon = b_1 \rho_e^2 \left(\frac{\rho_c}{\rho_e}\right)^{b_2} u_e\, \theta \tag{21}$$

Comparing this with Eq. (1), it is seen that a more reasonable reference density probably would have been ρ_c^2 rather than ρ_e^2.

6. NON-SIMILAR SOLUTION

Equation (21) is a plausible form for the eddy viscosity, which should be applicable at least to fully-developed, nearly adiabatic turbulent mixing for Mach numbers up to about 3. The justification for its use lies in the fact that experimental data correlate well with theory. Application of this equation at higher Mach numbers, for highly cooled mixing layers, or in the non-similar region close to the separation point (Fig. 1) obviously may be improper. Because of the urgent need for some sort of theoretical description of turbulent mixing under these conditions, however, the extended use of Eq. (21) is proposed. Any conclusions based on this model must of course remain tentative for conditions outside of the established correlation range.

We now propose to solve non-similar Eqs. (11) using Eq. (21) for the eddy viscosity. We introduce the correlation in the x coordinate transformation for the non-similar case.

$$S^* = F_w^{\,2} \int_0^x \rho_e u_e \mu_T r_o^{\,j}\, dx \tag{22a}$$

where

$$\mu_T \equiv \left[b_1 \left(\frac{\rho_c}{\rho_e} \right)^{b_2} \Phi \right] = k\, \Phi \tag{22b}$$

Comparing Eq. (22a) with the well-known laminar expression for S^*,[3] we see that the term μ_T replaces the laminar viscosity μ_e times $r_o^{\,j}$. Thus the relative growth rates dS^*/dx of turbulent and laminar mixing layers (in the two-dimensional case) are directly related by the ratio μ_T/μ_e. One sees that if the eddy viscosity is in fact representable by Eq. (21) over a wide range of conditions, then the density ratio

across the mixing layer (ρ_c/ρ_e) is extremely important in determining the growth of the turbulent mixing layer. It has already been shown that the conservation equations have been converted to laminar form in Eqs. (11). Eqs. (22) provide the transformation of S^* back to physical space. In essence what has been accomplished, therefore, is the placement of the turbulent effects into the coordinate transformations. One should thus be able to obtain universal solutions to Eq. (11) which depend only on the shape of the initial profile $F(0,u^*)$, just as in the laminar case.

The task that remains is to obtain the initial mixing layer profiles by solving the boundary layer on the body surface upstream of separation. Eqs. (11) will then be solved by a finite difference method.[2,3] The simplest case to consider is that for laminar flow on the body surface, which is a limiting situation which might correspond to the occurrence of transition at the separation point. A slightly more difficult but still tractable problem occurs for fully developed constant pressure turbulent flow (i.e. cone or wedge). The calculations of this report are restricted to these cases.

7. LAMINAR INITIAL CONDITIONS

For laminar flow on the body it is found that Blasius solution is applicable. Thus at the separation point:

$$F(0,u^*) = \frac{f''_B(u^*)}{\sqrt{2S_w}} \tag{23a}$$

$$u^* = f'_B(\eta_B) \tag{23b}$$

$$\eta_B = \frac{u_e r_o^{\,j}}{\sqrt{2S_w}} \int_o \rho dy \tag{23c}$$

$$S_w = \int_{body} C_b \rho_e u_e \mu_e r_o^{\,2j} dx \tag{23d}$$

$$C_b = \rho\mu/\rho_e\mu_e \text{ (Chapman-Rubesin constant for the body)} \tag{23e}$$

In (23a) and (23b) prime denotes differentiation with respect to the Blasius variable η_B. As in the laminar mixing case[2] we let:

$$F_w = f''_B(0)/\sqrt{2S_w} \tag{24a}$$

$$f''_B(0) = .4696 \tag{24b}$$

The initial condition for the energy equation is $W = 1-u^*$, since the Crocco integral is assumed to apply to the flow on the body surface.

8. TRANSFORMATION INVERSION - LAMINAR BODY

The calculation of S^* is now considered. From Eq. (22), we are led to the following differential equation:

$$\frac{dS^*}{dx} = \left[\rho_e u_e F_w k r_o^{\,j}\right] \Phi^* \tag{25a}$$

$$\Phi^*(S^*) \equiv F_w \Phi = \int_0^1 u^*(1-u^*) \frac{du^*}{F^*} \tag{25b}$$

Define a new variable x^* by the following relation

$$x^* = \int_0^x \rho_e u_e F_w k \; r_o^{\,j} dx \tag{26}$$

Then Eq. (25a) may be written

$$\frac{dS^*}{dx^*} = \Phi^*(S^*) \qquad S^*(0) = 0 \tag{27}$$

This equation was integrated using the function data for Φ^* from the shear layer solution, and the resulting function $x^*(S^*)$ is given in Fig. 14. The relation between S^* and physical x is therefore obtained from Eq. (26) and the function $x^*(S^*)$.

For comparison of turbulent mixing with the laminar mixing case, it may be desirable to express the turbulent solution in the laminar variables. For this we need to calculate S^{**} for the turbulent case, where

$$S^{**} \equiv S/S_w$$

$$S = \int_0 C_m \rho_e u_e \mu_e r_o^{\,2j} dx \tag{28}$$

and C_m is the laminar Chapman-Rubesin constant for the mixing layer. Then the rate of build-up of transformed length scale ratio S^{**} with respect to x^* is given by:

$$\frac{dS^{**}}{dx^*} = \left\{ \frac{C_m \mu_e}{k\ F_w S_w} \right\} r_o^{\ j} \tag{29}$$

The bracket term in Eq. (29) is a constant for a given body at given flow conditions. The value of this constant in a base flow depends on the details of the "matching," which is carried out using the Chapman-Korst recompression condition. For two dimensional flow the laminar length variable S^{**} is proportional to $x^*(S^*)$, but for axisymmetric flow the radius factor enters explicitely. Further discussion of the laminar-body, turbulent-mixing-layer problem is deferred until later.

9. TURBULENT INITIAL CONDITIONS

For a turbulent body boundary layer we need to obtain new initial conditions which replace Eq. (23) in the analysis of the preceding sections. In spite of the great effort which has been devoted to research on turbulent boundary layers, there still does not exist a well established theoretical method to obtain compressible turbulent boundary layer profiles. The most recent and promising method appears to be the transformation method of Coles,[17] as further explained by Crocco.[18] Thus a transformation will be found which (hopefully) establishes a correspondence between a known incompressible flow and the desired compressible flow. The incompressible profiles (which are established by a semi-empirical method) are thereby transformed to the compressible flow.

Let "barred" symbols refer to the transformed incompressible flow and unbarred symbols represent the compressible flow. The aim of the Coles transformation is to find the quantities $\sigma(x)$, $\eta(x)$, and $\xi(x)$ defined as follows:

$$\left(\frac{r_o}{\bar{r}_o}\right)^j \frac{\bar{\psi}(\bar{x},\bar{y})}{\psi(x,y)} = \sigma(x) \tag{30a}$$

$$\frac{\bar{\rho}}{\rho}\frac{\partial \bar{y}}{\partial y} = \eta(x) \tag{30b}$$

$$\frac{d\bar{x}}{dx} = \xi(x) \tag{30c}$$

where the stream functions are:

$$\bar{\psi} = \bar{r}_o^{\,j} \int_o^{\bar{y}} \bar{\rho}\bar{u}\, d\bar{y} \tag{30d}$$

$$\psi = r_o^{\,j} \int_o^{y} \rho u\, dy \tag{30e}$$

(The quantity of σ Eq. (30a) is not related to the jet-mixing σ of Fig. 4.) Restricting attention to the case of zero pressure gradient, Coles and Crocco find that

$$\frac{u}{\bar{u}} = \frac{u_e}{\bar{u}_e} = \frac{\eta}{\sigma} = \text{constant} \tag{31}$$

The relation between the wall shear stresses is

$$\frac{\bar{\tau}_w}{\tau_w} = \frac{\sigma}{\eta^2} \frac{\bar{\rho}_w \bar{\mu}_w}{\rho_w \mu_w} = \frac{\bar{C}_f \bar{\rho}_e \bar{u}_e^{\,2}}{C_f \rho_e u_e^{\,2}} \tag{32}$$

where $C_f \equiv \tau_w/(\rho_e u_e^{\,2}/2)$ is the usual skin friction coefficient. Coles introduces the idea of a turbulent substructure, which yields for σ the result

$$\sigma = \frac{\bar{\mu}}{\mu} \cdot \frac{\mu}{\mu_s} = \left(\frac{\bar{\mu}_w}{\mu_w}\right)\left(\frac{\mu_w}{\mu_s}\right) \tag{33}$$

where μ_s is a mean substructure viscosity, obtained from the hypothesis of a constant substructure Reynolds number.[17,18] From Eq. (31) to (33) we obtain

$$\sigma^2 \equiv \frac{C_f}{\bar{C}_f} = \left(\frac{\rho_w}{\rho_e}\right)\left(\frac{\mu_w}{\mu_s}\right) \tag{34}$$

For the case of $Pr_t = 1$ the Crocco integral relation holds on the body. Then if laminar viscosity is assumed proportional to static enthalpy, the following generalization of Coles' results (Coles' Eq. 4.17 for μ_s/μ_w is obtained:

$$\frac{\mu_s}{\mu_w} = 1 + \sqrt{\frac{\bar{C}_f}{2}}\left[a_1\left(\frac{H_e - H_w}{H_w}\right) - a_2\left(\frac{H_e - h_e}{H_w}\right)\sqrt{\frac{\bar{C}_f}{2}}\right] \tag{35a}$$

$$a_1 = 17.5 \qquad\qquad a_2 = 305 \tag{35b}$$

It is further consistent within this framework to use the approximation

$$\frac{\rho_e}{\rho_w} = \frac{H_w}{h_e} \tag{36}$$

So that from Eq. (34):

$$\frac{\bar{C}_f}{C_f} = \left\{\frac{H_w}{H_e} + \sqrt{\frac{\bar{C}_f}{2}}\left[a_1\left(\frac{H_e - H_w}{H_e}\right) - a_2\left(\frac{H_e - h_e}{H_e}\right)\sqrt{\frac{\bar{C}_f}{2}}\right]\right\}\left(\frac{H_e}{h_e}\right) \tag{37}$$

The simplest way to treat the compressible turbulent boundary layer using this formulation is to specify $\bar{C}_f$ (i.e. work the problem backwards by specifying the equivalent incompressible skin friction coefficient). Then the compressible skin friction is given by Eq. (37), and the compressible heat transfer is obtained from the enthalpy gradient using the Crocco integral. What remains to be done, then, is to find the relation between the compressible and incompressible length scales (i.e. Reynolds numbers). Then the compressible velocity profile can be expressed in terms of a given incompressible profile corresponding to the specified $\bar{C}_f$.

Rather than finding the relation for $\xi(x)$, we instead seek a direct relation between $\bar{C}_f$ and the compressible length x. If the Coles-Crocco

transformation relations are substituted in the compressible momentum integral relation, it is found that

$$d\tilde{x} \equiv \rho_w u_e r_o^{\,j} dx = \left(\frac{2}{\bar{C}_f}\right)\left(\frac{\mu_s}{\mu_w}\right) d\left\{r_o^{\,j}\mu_w\left(\frac{\mu_s}{\mu_w}\right)\bar{R}_{e_\theta}\right\} \tag{38a}$$

$$\bar{R}_{e_\theta} \equiv \frac{\bar{\rho}_e \bar{u}_e}{\bar{\mu}} \int_0^\infty \bar{u}^* \left(1 - \bar{u}^*\right) d\bar{y} \tag{38b}$$

The incompressible momentum thickness Reynolds number $\bar{R}_{e_\theta}$ is related to $\bar{C}_f$ by a relation based on the law of the wall. Let the incompressible velocity profile in this region be given by (Ref. 19, page 140):

$$\frac{\bar{u}}{\bar{u}_\tau} = \frac{1}{k}\,\ell n\,\frac{\bar{u}_\tau \bar{y}}{\bar{\nu}} + C \tag{39a}$$

$$\bar{u}_\tau \equiv \sqrt{\frac{\tau_w}{\bar{\rho}}} = \bar{u}_e\sqrt{\frac{\bar{C}_f}{2}} \tag{39b}$$

where according to Coles,[20] $K = .4$ and $C = 5.1$. Then from Eq. (38b) it is found that

$$\bar{R}_{e_\theta} = \frac{e^{-KC}}{K}\left\{e^Z\left(1 - \frac{2}{Z}\right) + \left(1 + \frac{2}{Z}\right)\right\} \tag{40a}$$

where

$$Z \equiv \frac{K}{\sqrt{\bar{C}_f/2}} \tag{40b}$$

By using Eq. (40) and (35), Eq. (38) can be integrated along the body from the point of transition to the base. If Z is assumed to be very large, then the integration is easy to carry out. Assuming that transition occurs at the nose, the final result may be put into the standard form:

$$\frac{\varphi}{\sqrt{C_f}} = C_1 + C_2 \log_{10} \left[\frac{H_w \mu_w}{h_e \mu_s} C_f \tilde{R}_{e_T} \right] \tag{41a}$$

where φ is defined in Eq. (34) and

$$C_1 = \frac{KC + \ln K}{K\sqrt{2}} \approx 1.99 \tag{41b}$$

$$C_2 = \frac{\ln (10)}{K\sqrt{2}} \approx 4.07 \tag{41c}$$

$$\tilde{R}_{e_T} = \frac{\int_0^x \rho_w u_e r_o^j dx}{\mu_w r_o^j} \equiv \frac{\tilde{x}}{\mu_w r_o^j} \tag{41d}$$

Equations (35), (37), and (41) are three equations for the three unknowns C_f, $\bar{C}_f$, $\frac{\mu_w}{\mu_s}$. The parameters are H_w/H_e, $H_e = h_e$, and $\tilde{R}_{e_T}$, which will be known for a given body at given flight conditions.

For wedges and cones Eq. (41d) may be integrated explicitely. Figs. 6, 7 and 8 show values of the equivalent $\bar{C}_f$ for these bodies as a function of wall enthalpy ratio, boundary layer edge Mach number M_2 or enthalpy ratio H_e/h_e, and reduced Reynolds number $\tilde{R}$:

$$\tilde{R} = \frac{C_w \, Re_2}{j + 1} \tag{42a}$$

$$R_{e_2} = \frac{\rho_e u_e x_{base}}{\mu_e} \tag{42b}$$

$$C_w = \rho_w \mu_w / \rho_e \mu_e \tag{42c}$$

From the result for $\bar{C}_f$, the initial compressible $F(u^*)$ profile at the body base can be found from the laminar sublayer and law-of-the-wall profiles. Thus:

$$\text{Sublayer:} \quad F = F_w = \frac{\bar{C}_f}{2}\left(\frac{\mu_w}{\mu_s}\right)\frac{1}{\mu_w r_o j} \tag{43a}$$

in the region

$$0 \le u^* \le u^+ \sqrt{\bar{C}_f/2} \tag{43b}$$

Rubesin[21] finds that $u^+ = 13.1$. In the law-of-the-wall region the velocity gradient function is found from Eq. (39) and the properties of the Coles-Crocco transformation:

$$\text{Law-of-the-wall:} \quad F = \frac{F_w}{K}\exp\left[-K\left[\frac{u^*}{\sqrt{\bar{C}_f/2}} - \bar{C}\right]\right] \tag{43c}$$

in the region

$$u^+ \sqrt{\bar{C}_f/2} < u^* < 1 \tag{43d}$$

In this form the initial velocity gradient profile F/F_w is a function only of the equivalent incompressible skin friction coefficient $\bar{C}_f$. Therefore this is the natural parameter defining a family of solutions to the non-similar turbulent mixing layer problem. Fig. 9 shows the shape of these profiles for various values of $\bar{C}_f$ in the range of interest. One sees that there are square corners at locations corresponding to the sublayer limit, and the outer edge. This behavior is, of course, not physically reasonable, so these points should be arbitrarily rounded slightly to obtain a reasonably smooth starting profile for the non-similar mixing layer calculation. This hopefully will not affect the dividing streamline properties much because the dividing streamline is initially at $u^* = 0$. One could probably improve the profile by including the law-of-the-wake and buffer layers, but this does not seem worth the effort at present. The discontinuity at $S^* = u^* = 0$ (i.e. $F(0) = 0$ immediately after separation) is of course treated in the same manner as done in the laminar case.[22]

Note that for a base flow problem the sudden turn at the separation point causes a distortion of the profile. If one assumes that this occurs according to an isentropic expansion along streamlines (as in Ref. 23), then one could use the distorted initial profiles as the mixing layer initial conditions. This would involve finding the streamlines using the Coles-Crocco relation for the stream function from Eq. (30) and presents no essential difficulty. The presumed increase in accuracy from this refinement does not appear to be worth the effort at this stage, but can be included in a later analysis if the present results appear promising.

For the turbulent body and turbulent-mixing-layer problem, then, the initial conditions are given by:

$$F^* = \begin{cases} 1 & 0 < u^* < 13.1\sqrt{\bar{C}_f/2} \quad (44a) \\ \frac{1}{.4}\exp\left\{-.4\left[\frac{u^*}{\sqrt{\bar{C}_f/2}} - 5.1\right]\right\} & 13.1\sqrt{\bar{C}_f/2} < u^* < 1 \quad (44b) \end{cases}$$

The integration procedure is again identical to the purely laminar case. The non-similar calculation of the shear layer must of course be repeated because the turbulent initial profile shapes are different.

10. TRANSFORMATION INVERSION - TURBULENT BODY

As before, one needs to know the relation between S^* and the physical length x. Also for comparison with the purely laminar results it may be desirable to know the solution in terms of the laminar streamwise scale parameter $S^{**} = S/S_w$. Examination of the transformation equations reveals that the rate of build-up of S^{**} along the shear layer is given by Eq. (29), with $x^*(S^*)$ defined by Eq. (27). Thus the difference between turbulent mixing cases having laminar or turbulent initial conditions resides only in the shape of the initial profile and in the value of wall velocity gradient at separation F_w. For the laminar body this quantity is given by Eq. (24), while for the turbulent body it is obtained from Eq. (43a).

11. NUMERICAL SHEAR LAYER CALCULATIONS

Non-similar shear layer calculations were carried out corresponding to the three turbulent initial profiles and the laminar profile shown in Fig. 9. The calculations were started at $S^* = 10^{-6}$ and carried to $S^* = 10^3$, with output at intervals of 0.2 in $\log_{10}(S^*)$. Approximately ten minutes of IBM 7094 time was required for each initial profile. The u^* mesh contained 80 intervals in the range $0 \leq u^* \leq .05$ and 152 intervals in the remaining range $.05 \leq u^* \leq 1.0$. Overall integral balances (from momentum and energy) agreed within 0.5°/o for all conditions, which is probably indicative of the accuracy of the numerical calculations.

Fig. 10 shows the results of the non-similar shear layer calculations for the velocity gradient function F^* for the four different initial profiles shown in Fig. 9. This is the solution of Eq. (11a). At small values of the streamwise variable S^* the profiles resemble the initial conditions, but as S^* increases the profiles become more rounded and decay in amplitude. This is of course to be expected since the differential equation is parabolic. One would expect that as $S^* \to \infty$ the shape of the F^* curves would approach the asymptotic shape given by the Chapman profile. Because of computer cost, however, it was necessary to stop the calculation at $S^* = 10^3$. Only the Blasius (and perhaps the $\bar{C}_f = .006$) profile were near the asymptotic shape at this value of S^*.

The solution for the enthalpy function W from Eq. (11b) is shown in Fig. 11. Because the Crocco integral for total enthalpy is assumed to be valid initially, $W = 1 - u^*$ for all profiles at the initial station. Since the W equation is also parabolic, the decay of this function is qualitatively similar to the F^* curves. Differences in W results for

the various initial F^* profiles do not become apparent, however, until some distance downstream ($S^* \approx 10^{-2}$) because all W profiles begin with the same initial condition. At large S^* one would again expect the shape of the W function curves to be independent of the initial F^* profile shape, but this occurs at $S^* > 10^3$.

Fig. 12 shows the results for the velocity u_D^* on the dividing streamline, as obtained by integrating the momentum equation for $v = 0$.[2]

$$u_D^* \frac{du_D^*}{dS^*} = F_D^* \left(\frac{\partial F^*}{\partial u^*}\right)_D \tag{45}$$

For the Blasius and $\bar{C}_f = .006$ initial profiles u_D^* has effectively reached the Chapman limiting value of .587 at $S^* = 10^3$, but the other profiles apparently require several more decades in S^* to reach the limit. All the initial profiles used give the same value of u^* for small S^*, since the starting profiles of Baum[22] (small S^* and u^*) are identical, as may be seen from Fig. 9.

The development with distance of the enthalpy function W_D on the dividing streamline is illustrated in Fig. 13. The limiting value $W_D = .611$ as $S^* \to 0$ was obtained from the starting solution of Baum.[22] At large S^* the W function decays uniformly to zero (Fig. 11), but at $S^* = 10^3$, W_D still has an appreciable magnitude for the $\bar{C}_f = .004$ and .006 initial profiles.

It should be noted that a direct comparison between the laminar and turbulent cases cannot be made on the basis of Fig. 10-13, since the streamwise variable S^* is not directly related to the streamwise distance. For this one must use the variables x^* or S^{**} for the turbulent shear layer, or better yet the actual distance x. The relation between x^* and S^* from Eq. (27) is shown in Fig. 14. Fig. 15 gives values of the momentum thickness integral $\Phi^*(S^*)$ which appears in Eq. (27).

12. BASE FLOW OF CONE OR WEDGE

Fig. 16 illustrates the application of the mixing layer analysis to the base flow region. The "core" or recirculating region is assumed to have negligible velocity and constant (but initially unknown) enthalpy H_c. The recompression region is assumed to be small, and recompression is assumed to be isentropic along streamlines. The distortion of the initial profiles at separation is neglected, although it could be included later using the method of Ref. 23.

Following the previous laminar analysis,[2,3] the configuration of the base flow is determined using the empirical Chapman-Korst recompression condition. This states that the total pressure on the stagnating streamline just before recompression must equal the static pressure after recompression (determined from the inviscid flow calculation). Assuming that the values of u^* and W on the dividing streamline are available (from Figs. 12 and 13), matching involves the simultaneous calculation of the inviscid flow (as defined by the initial wake angle), the core enthalpy H_c, the value of S^* corresponding to the position of recompression, and possibly the total base heat transfer rate Q_b. As shown in Refs. 3 and 11 these latter quantities are related by an overall energy balance condition.

By equating the energy entering the base region through the body boundary layer to that leaving through the neck and by base heat transfer, the following equation is obtained:[3,11]

$$H_c = H_e - \frac{H_e Q^*_b + (H_e - H_w)\,(K^* - J^*)}{L^*} \tag{46a}$$

where

$$Q^*_b = \frac{Q_b F_w}{H_e (2\pi) j} \tag{46b}$$

$$K^* = \left[\int_0^1 \frac{u^*(1-u^*)}{F^*}\, du^*\right]_{body} = \Phi^*(0) \tag{46c}$$

$$J^* = \left[\int_{u_s^*}^1 \frac{u^* W}{F^*}\, du^*\right]_{recompression} \tag{46d}$$

$$L^* = \left[\int_{u_s^*}^1 \frac{u^*(1-u^*-W)}{F^*}\right]_{recompression} \tag{46e}$$

and u_s^* is the velocity on the stagnating streamline just before recompression. It may be seen that Eq. (46a) is a relation between H_c, Q_b, and S_s^*, the value of S^* defining the position of recompression.

Because the base heat transfer Q_b enters into the matching analysis, one needs an additional relation which specifies this quantity. Probably Q_b is proportional to the enthalpy difference $(H_c - H_b)$, where H_b is the enthalpy corresponding to the base wall temperature. An analysis of the laminar case[24] showed that conditions were such that Q_b could safely be assumed to be zero without affecting the base flow solution much. For the time being it is assumed that this conclusion is valid for turbulent flow as well, so that in what follows the assumption $Q_b = 0$ is made.

In order to compare the turbulent base flow results with laminar results, matching calculations were carried out for a 10° cone for perfect gas conditions with $\gamma = 1.4$ and viscosity proportion to temperature to the .76 power. For simplicity the outer edge conditions in the base region were obtained from a Prandtl-Meyer expansion at the corner, and the shear layer was assumed to be straight between separation and recompression. The recompression was assumed to be isentropic and all

Chapman-Rubesin constants were assumed to be equal to unity. This model corresponds to calculations previously carried out for the laminar case.[25] Details of the numerical procedure for carrying out matching calculations were given in Ref. 11.

13. RESULTS FOR 10° CONE

Even with the approximations listed in the previous section, the base flow results are a function of Mach number, Reynolds number, body shape, wall enthalpy ratio, and condition of the boundary layer at the separation point. Because of the preliminary nature of the present theory for turbulent flow, it does not seem appropriate to make an exhaustive study of the effects of each variable at this time. Instead, attention is restricted mainly to a 10° half-angle cone with a "highly-cooled" surface. The results therefore will indicate how the theory, developed from a correlation of experimental data at low supersonic speeds, is extrapolated to conditions typical of re-entry conditions on a slender body.

Figure 17 shows the effect of Mach number on the dividing streamline velocity just before recompression for a cold-wall 10° cone at $Re_1 = 10^6$. The curve labeled "turbulent" corresponds to a fully developed turbulent flow on the body surface and a turbulent mixing layer. The laminar curve gives the results previously reported for completely laminar flow,[25] while the "laminar-turbulent" curve is based on the assumption of a laminar body and turbulent mixing layer (i.e. transition at the separation point). One sees that at high Mach numbers all curves give a dividing streamline velocity in the range 0.2 to 0.3, which is very much lower than the Chapman value of .587. This indicates that the mixing layer in the base flow undergoes recompression long before the fully developed or asymptotic condition is approached. At low Mach numbers, however, the turbulent u_D^* curves approach $u^* = .587$, indicating that at lower Mach numbers the turbulent mixing effect (as measured by the eddy viscosity ϵ) is very much stronger. The strong Mach number effect on ϵ is directly related to the effect of Mach number on the eddy viscosity factor k of Fig. 5. In fact, the effect of Mach

number on k completely overshadows the effect of Mach on the initial profile shape. Thus from Fig. 6 it is seen that reducing the Mach number reduces $\bar{C}_f$ while Fig. 12 shows that this reduces the rate of build-up of dividing streamline velocity u_D^*. Because the expression for k completely dominates the analysis, experiments are needed to see if the trend of Fig. 5 persists to high Mach number conditions.

Figure 18 shows the results of the energy balance to determine the enthalpy H_c in the recirculating core region. Again the effect of Mach number is evident, the results indicating that at low Mach numbers the turbulent mixing is so rapid that $H_c \rightarrow H_e$, i.e. adiabatic conditions. This occurs in spite of the fact that the upstream body surface is highly cooled. Any base heat transfer would of course tend to lower H_c, and this may be an important effect in turbulent flow. If the proposed correlation for k of Fig. 5 is correct, then the core enthalpy may be extremely important, since for a perfect gas:

$$k \approx .0606 \left(\frac{\rho_c}{\rho_e}\right)^{2.0} \approx .0606 \left(\frac{h_e}{H_c}\right)^{2.0} \tag{47}$$

The core enthalpy therefore enters into the determination of the eddy viscosity.

The calculated effects of Mach and Reynolds numbers on the centerline stagnation enthalpy at recompression are shown in Figs. 19 and 20. The results for h_s/H_e as a function of Mach number closely follow those for the core enthalpy. At high Mach numbers the turbulent results are far from adiabatic, and the theory even predicts a decrease in h_s/H_e if transition occurs in the mixing layer at Re_1 less than 10^7 (Fig. 20). Since the "fast expansion" distortion of the initial profiles has been neglected in these calculations, h_s might even be smaller due to this effect, if the laminar results[23] carry over to the turbulent case.

Finally, the effect of Mach and Reynolds numbers on the base pressure is indicated in Figs. 21 and 22. Generally speaking, the range of P_b/P_∞

is about .3 to .6, regardless of conditions. One notices that at high Mach numbers the laminar and turbulent predictions appear to agree within about $15^{o}/o$. If the theory can be believed under these conditions, then one should not expect transition in the base flow of a slender re-entry vehicle to be accompanied by a large change in base pressure. This is in contrast to the situation for Mach 3 adiabatic conditions (shown in Fig. 22), where a sudden drop in base pressure is indicated as the flow changes from laminar to turbulent.

14. CONCLUDING REMARKS

In the present report a new empirical turbulent mixing and base flow model has been constructed which hopefully will be applicable slender re-entry vehicles. A plausible method has been found to extrapolate turbulent mixing results for low Mach numbers to high Mach number flows and to include the effects of non-similar and highly cooled turbulent mixing layer development. Reasonable results were found for gross effects such as the base pressure and rear stagnation enthalpy for a highly cooled 10° half-angle cone.

The asymptotic mixing layer analysis for adiabatic conditions up to about Mach 3 can probably be considered reasonable, since the velocity profile data appear to be correlated. Under these conditions the effect of any initial boundary layer thickness becomes negligible, since the turbulent profiles develop very rapidly. Application of the present theory to any situation where the initial profile effects may become important must be considered conjecture at this stage, since no experimental confirmation is presently available. This includes the highly cooled case at relatively low Mach numbers and all conditions at high Mach numbers. Hopefully, the present treatment of non-similar turbulent mixing can serve as a guide to future experiments for these technically important flow conditions.

REFERENCES

1. F.L. Fernandez, J.L. Carson, D.A. Anderson — "Wake Radar Cross Section of Slender Re-Entry Vehicles," Aerospace Corporation, Rept. BSD-TD-64-152, Oct. 1964.

2. M.R. Denison, E. Baum — "Compressible Free Shear Layer with Finite Initial Thickness," AIAA Journal 1, 342, Feb. 1963.

3. E. Baum, H.H. King, M.R. Denison — "Recent Studies of the Laminar Base-Flow Region," AIAA Journal 2, 1527, Sept. 1964.

4. B.L. Reeves, L. Lees — "Theory of the Laminar Near Wake of Blunt Bodies in Hypersonic Flow," AIAA Paper No. 65-52, Jan. 1965.

5. W.H. Webb, R. Golik, L. Lees — "Preliminary Study of the Viscous Inviscid Interaction in the Laminar Supersonic Near Wake," TRW Space Tech. Labs., Rept. BSD-TDR-64-114, July, 1964.

6. A. Mager — "Transformation of the Compressible Turbulent Boundary Layer," Jour. of Aero. Sci. 25, 305, May 1958.

7. O.R. Burggraf — "The Compressibility Transformation the Turbulent-Boundary-Layer Equations," Jour. Aero. Sci. 29, 434, April 1962.

8. L. Ting, P.A. Libby — "Remarks on the Eddy Viscosity in Compressible Mixing Flows," Jour. of the Aero. Sci. 27, 747, Oct. 1960.

9. H. Schlichting — Boundary Layer Theory, Chapter XXIII, Pergamon Press, New York, 1955.

10. A. Ferri, P.A. Libby, V. Zakkay — "Theoretical and Experimental Investigation of Supersonic Combustion, Proc. of the 3rd Congress of the International Council of the Aeronautical Sciences, Paper No. 51, Spartan Books, Inc., Wash., D.C., 1964.

11. H.H. King, E. Baum — "Enthalpy and Atom Profiles in the Laminar Separated Shear Layer," Electro-Optical Systems Res. Note RN-8, March 1963.

12. D.R. Chapman — "A Theoretical Analysis of Heat Transfer in Regions of Separated Flow," NACA TN 3792, Oct. 1956.

13. W.J. Christian — "Improved Numerical Solution of the Blasius Problem with Three-Point Boundary Conditions," Jour. of Aero. Sci. 28, 911, Nov. 1961.

14. R.C. Maydew, J.F. Reed — "Turbulent Mixing of Axisymmetric Compressible Jets (In the Half-Jet Region) with Quiescent Air," Sandia Corporation, Res. Rept. SC-4763(RR), March 1963.

15. H.W. Leipmann, J. Laufer — "Investigations of Free Turbulent Mixing," NACA TN 1257, Aug. 1947.

16. L.J. Crane — "The Laminar and Turbulent Mixing of Jets of Compressible Fluid," Jour. Fluid Mech., 3, Part I, Oct. 1957.

17. D.E. Coles — "The Turbulent Boundary Layer in a Compressible Fluid," Rand Corp., Rept. R-403-PR, 1962.

18. L. Crocco — "Transformations of the Compressible Turbulent Boundary Layer with Heat Exchange," AIAA Jour. 1, 2723, Dec. 1963.

19. C.C. Lin (editor) — Turbulent Flows and Heat Transfer, Vol. V, High Speed Aerodynamics and Jet Propulsion, Princeton Univ. Press, Princeton, New Jersey, 1959.

20. D.E. Coles — "The Law of the Wake in the Turbulent Boundary Layer," Jour. Fluid Mech. 1, Part 2, 191, July 1956.

21. M.W. Rubesin — "An Analytical Estimation of the Effect of Transpiration Cooling on the Heat-Transfer and Skin-Friction Characteristics of a Compressible, Turbulent Boundary Layer," NACA TN 3341, Dec. 1954.

22. E. Baum "Initial Development of the Laminar Separated Shear Layer," AIAA Jour. 2, 128, Jan. 1964.

23. E. Baum "Effect of Boundary Layer Distortion at Separation on the Laminar Base Flow," Electro-Optical Systems Res. Note RN-16, Oct. 1963.

24. H.H. King "An Analysis of Base Heat Transfer in Laminar Flow," Electro-Optical Systems Res. Note RN-14, Sept. 1963.

25. H.H. King "A Tabulation of Base Flow Properties for Cones and Wedges," Electro-Optical Systems Res. Note RN-17, Jan. 1964.

APPENDIX A

Maydew-Reed Dividing Streamline Location

Referring to Fig. 2, it may be seen that the total mass flow inside the dividing streamline at some station x downstream of the nozzle exit must equal the mass flow through the nozzle. Assuming that the flow is axisymmetric, the mass balance yields

$$\dot{M} \approx \left[\rho_e u_e A\right]_{exit} = \left[2\pi \int_0^{r_{DSL}} \rho u \, r \, dr\right]_x \qquad \text{(A-1)}$$

The total mass flow $\dot{M}$ through the nozzle was calculated by assuming an isentropic expansion from the reservoir conditions tabulated by Maydew and Reed[14] for each run.

Since the experimental porfile data u(r) are given by Maydew and Reed for each station x, the integral of Eq. (A-1) can be evaluated as a function of its upper limit until Eq. (A-1) is satisfied. This of course requires that the density variation be known, and this was assumed to be given by the Crocco integral relation for a perfect gas, Eq. (18). The dividing streamline velocity is then given by $u(r_{DSL})$.

An estimate of the accuracy of this procedure can be obtained by assuming that the flow inside the dividing streamline can be arbitrarily divided into a "profile" part and a "potential core" part. If most of the total $\dot{M}$ is in the potential core (as it is for small x), then a small error in the value of total $\dot{M}$ will have a large effect on the value of u_{DSL}. For example, at x = 1.5" a 5°/o change in $\dot{M}$ would produce about 50 to 100°/o change in u_{DSL} for the experimental conditions but at x = 9" a 5°/o change in $\dot{M}$ would produce only a 5°/o to 15°/o in u_{DSL}. The data shown in Fig. 3 for x = 1.5 and 3.0 inches therefore could be considerably in error.

APPENDIX B

Eddy Viscosity Factor k of Figure 5

When detailed profile data are available, as in the Maydew-Reed report, the factor k in the eddy viscosity expression (Eq. 1) can be found by a least-squares fit of the data with Eq. (19). However, much of the previous literature on the mixing problem does not contain sufficiently detailed profile data, but presents only the final result in the form of the jet spread parameter σ. A summary of previous experimental determinations of σ up to 1962 is given by Maydew and Reed. Since σ depends on the choice of profile used in the theory, this must also be specified.

One way that the quantity k can be related to σ is by comparing the derivatives $du^*/d(y/x)$ of Eq. (17) and (19) at some selected value of u^*. For example, for the error function profile

$$u^* = 1/2 \left(1 - \frac{2}{\sqrt{\pi}} \int_0^{\sigma y/x} e^{-z^2} dz\right) \qquad \text{(A-2)}$$

we match the slopes at $u^* = .5$ to get:

$$k = \frac{\sqrt{\pi}}{\sigma c \left(\frac{H_e}{h_e}\right) \left\{ \left[\frac{H_c}{H_e} - \left(1 - \frac{H_c}{H_e}\right) f_\eta - \left(1 - \frac{h_e}{H_e}\right) f_\eta^{\,2} \right] \frac{1}{f_{\eta\eta}} \right\}_{u^* = .5}} \qquad \text{(A-3)}$$

Thus one must specify the profile shape function $g(\sigma y/x)$ and the value of u^* at which the slopes are to be matched.

Clearly the above method for determining k may not be very accurate and in addition depends on an arbitrary assumption of the value of u^* at which the equation is evaluated. This procedure therefore will not

be used in this report, with one exception: The data of Zumwalt at Mach 3 referred to by Maydew and Reed provide an additional point on Fig. 5 which further extends the correlation.

In a private communication with Prof. Zumwalt at the University of Oklahoma it was found for the error function profile the best σ was roughly $\sigma \approx 23$ to 30 at Mach 2.9, depending on how the initial boundary layer thickness was taken into account. Eq. (A-3) was evaluated at $u^* = .5$ using this information to give the data points of Fig. 5 attributed to Zumwalt.

A second point to be made concerns the determination of k by correlating mixing layer profile data in the non-similar growth region. This will surely be a problem in high Mach number flows if the relation of Fig. 5 is approximately correct. The mixing layer experiment should produce either velocity or density profiles (or both) as a function of physical x and y. The basic equations of this report show that the theoretical relation for $u^*(x,y,k)$ is given implicitely by the relations:

$$y - y_{DSL} = \frac{1}{\rho_e u_e r_o^{\,j} F_w} \int_{u^*_{DSL}} \frac{\rho_e}{\rho} \frac{du^*}{F^*}$$

$$F^* = F^*(S^*, u^*)$$

$$S^* = S^*(x^*, \bar{C}_f)$$

$$\bar{C}_f = \bar{C}_f\,(H_w/H_e,\ h_e/H_e,\ R_e)$$

$$x^* = \int_0^x \rho_e u_e F_w\, k\, r_o^{\,j} dx$$

$$F_w = F_w\,(\bar{C}_f,\ H_w/H_e,\ h_e/H_e,\ \mu_w)$$

$$\rho = \rho(P, h)$$

$$h = H - u^2/2$$

Thus k appears explicitely in the relation for x^* as a function of x. Although somewhat cumbersome, these relations can be programmmed for a computer so that a least squares determination of k from velocity profile data, density profile data, or both can be performed.

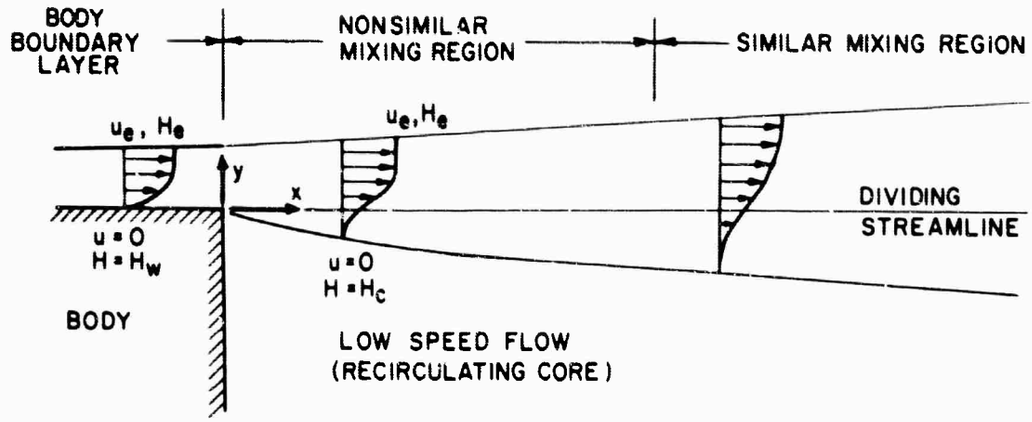

FIG. 1 MIXING LAYER REGIONS

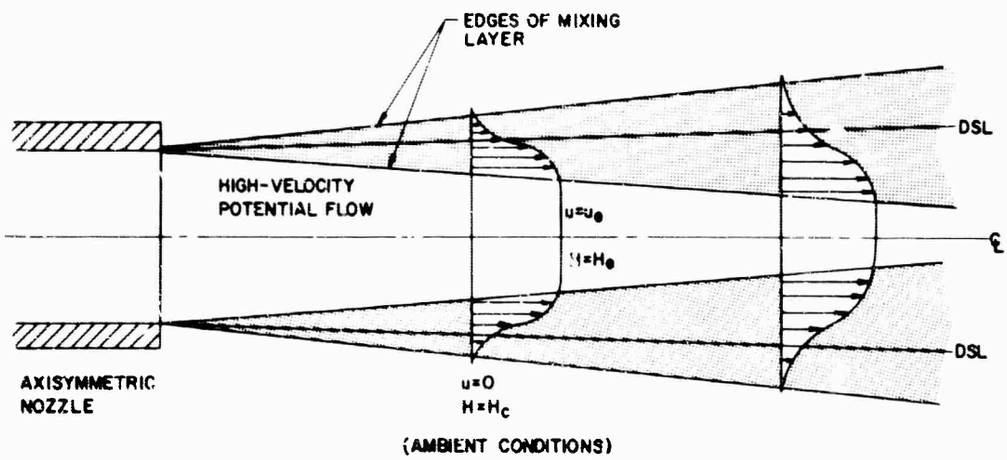

FIG. 2 GEOMETRY OF THE JET MIXING EXPERIMENT

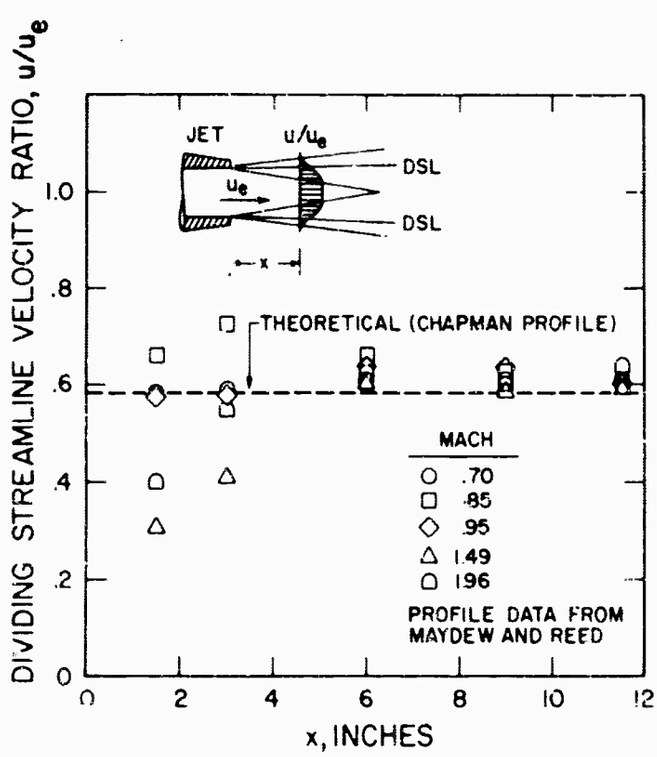

FIG. 3

EXPERIMENTAL DIVIDING STREAMLINE VELOCITY CALCULATED FROM MASS BALANCE

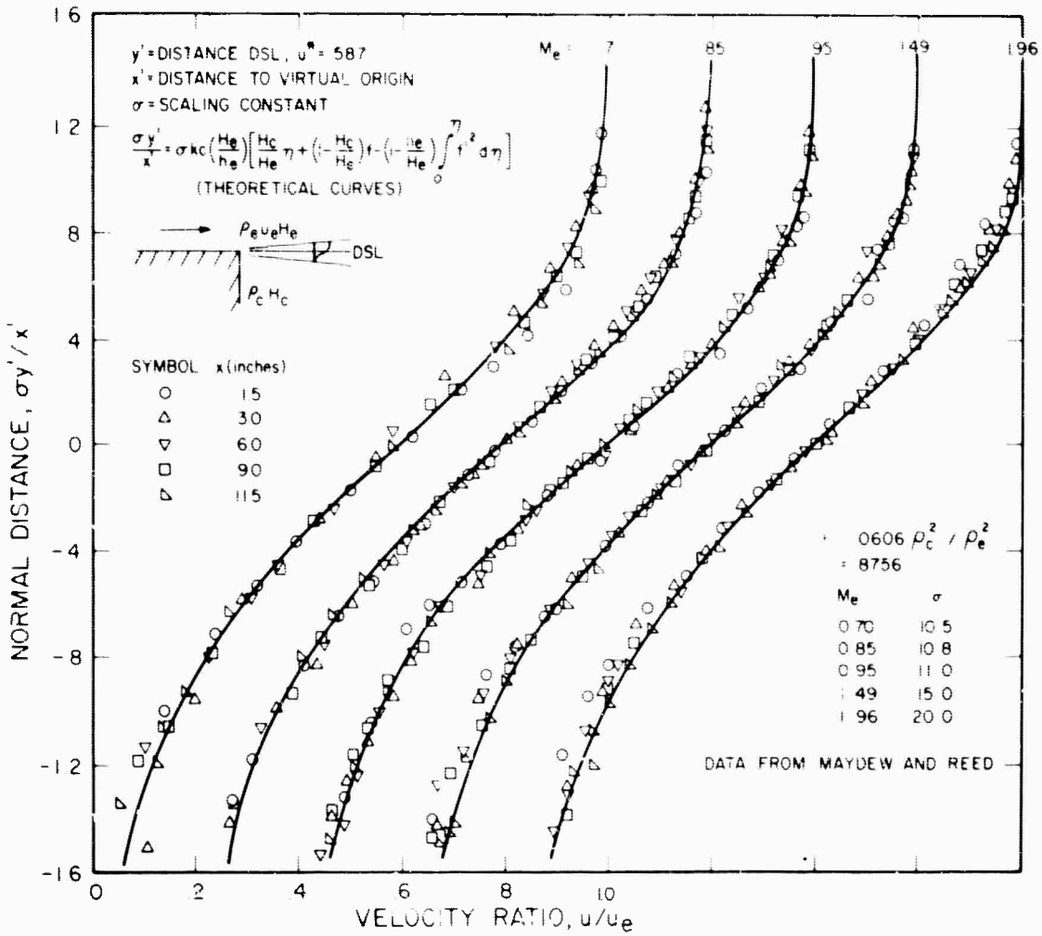

FIG. 4 CORRELATION OF PROFILE DATA

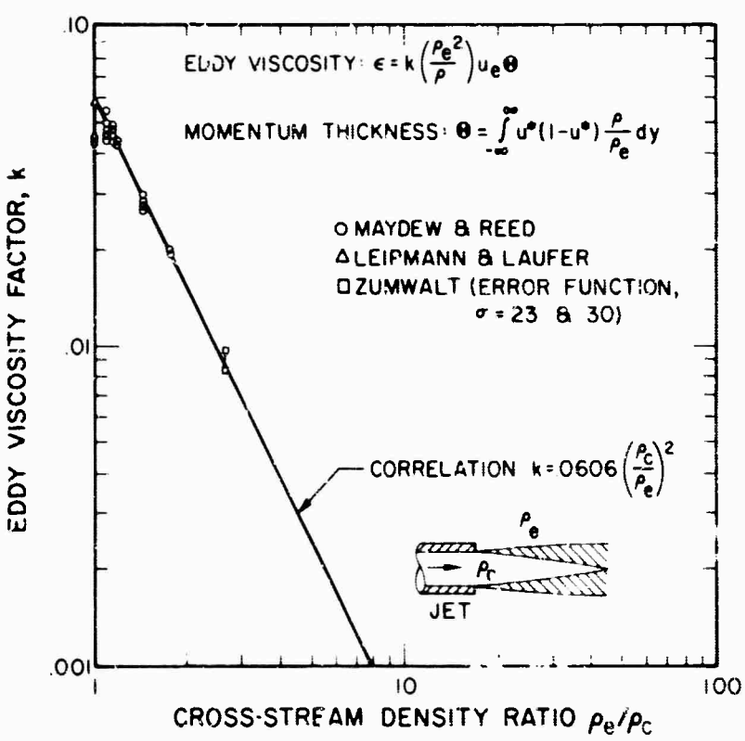

FIG. 5

CORRELATION TO DETERMINE THE EDDY VISCOSITY FACTOR k

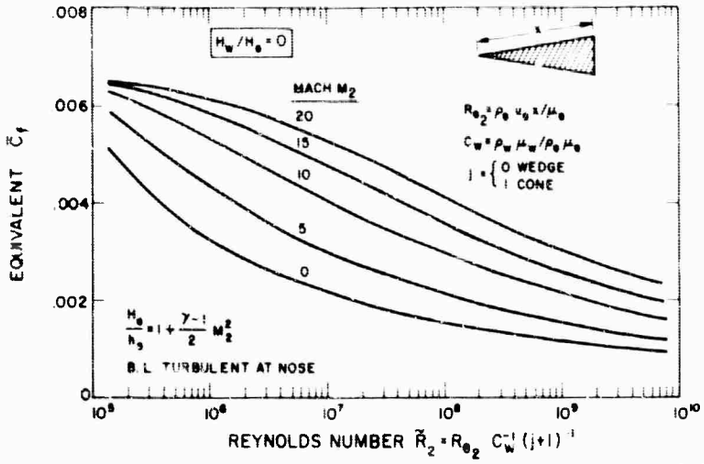

FIG. 6

EQUIVALENT SKIN FRICTION COEFFICIENT $\bar{C}_f$ FOR CONES AND WEDGES, $H_w/H_e = 0$

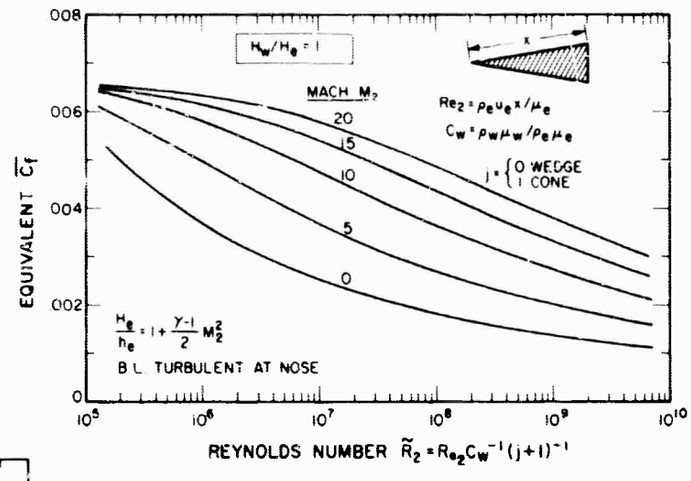

FIG. 7

EQUIVALENT SKIN FRICTION COEFFICIENT $\bar{C}_f$ FOR CONES AND WEDGES, $H_w/H_e = 1$

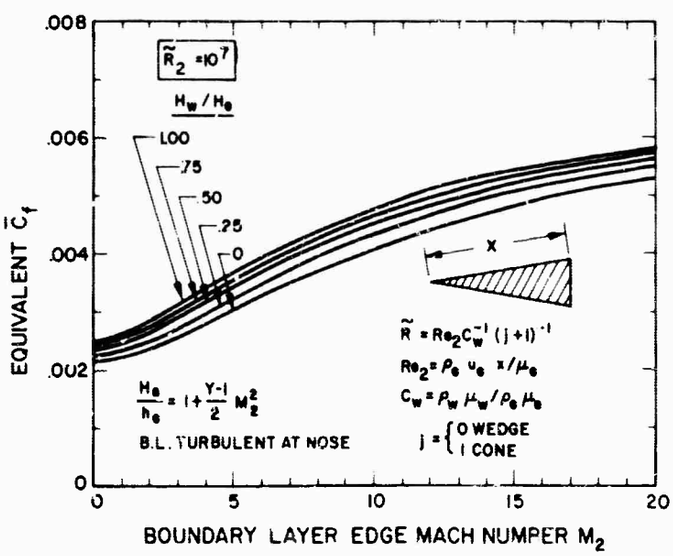

FIG. 8

EFFECT OF WALL ENTHALPY RATIO ON $\bar{C}_f$ FOR $\tilde{R} = 10^7$

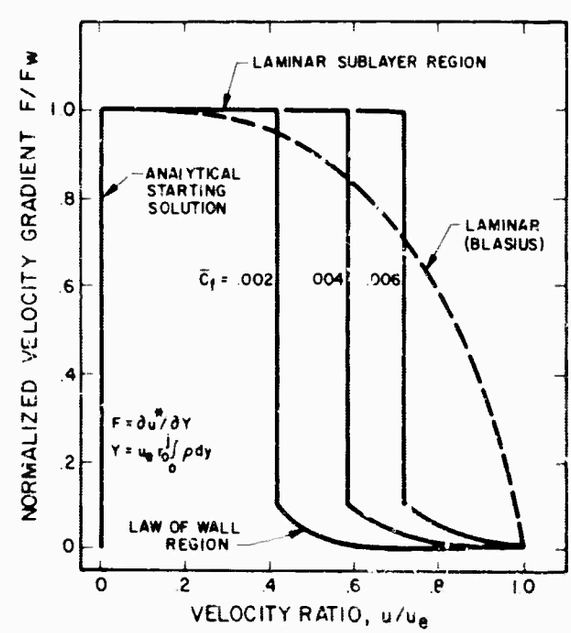

FIG. 9

TURBULENT INITIAL MIXING LAYER PROFILE

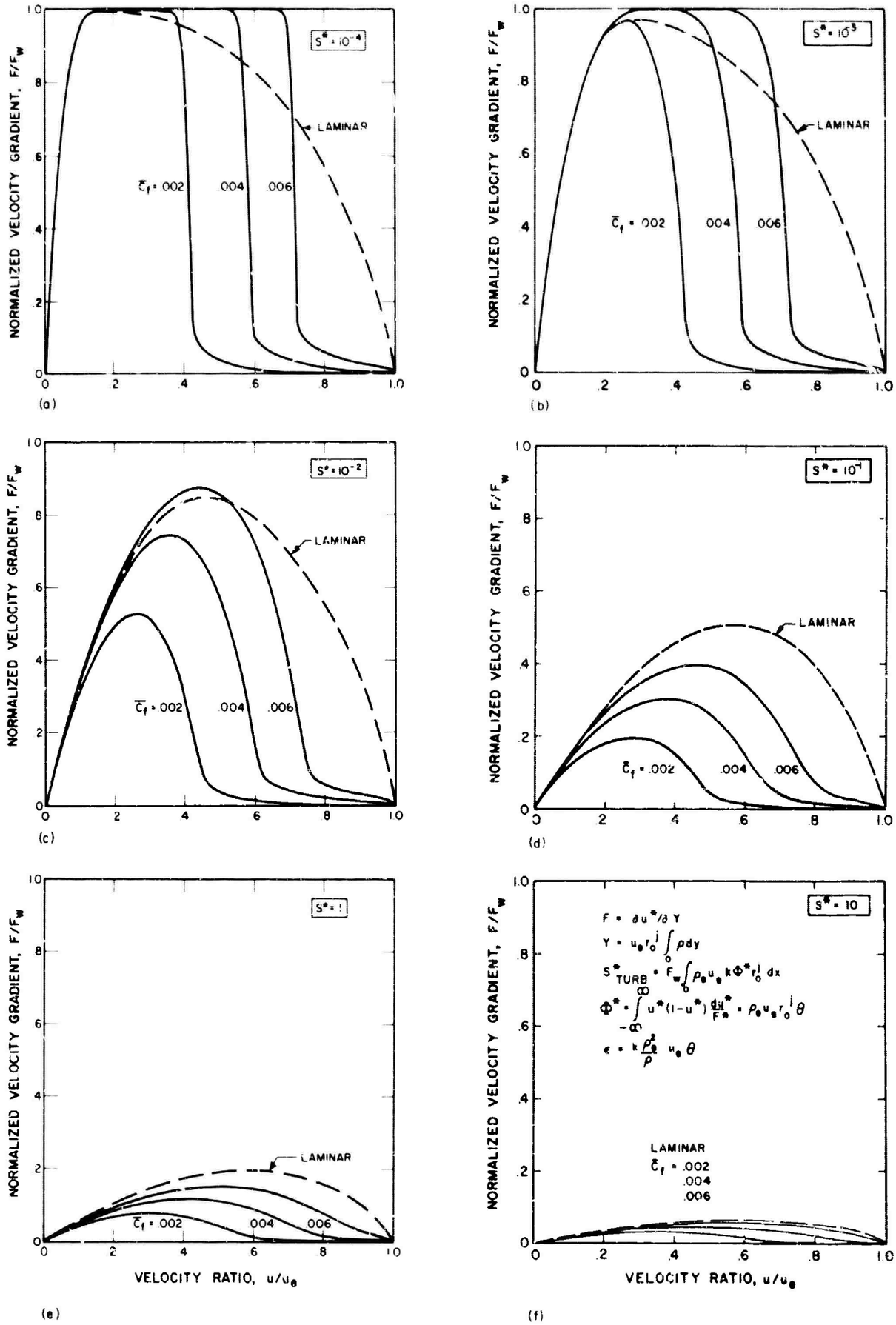

FIG. 10 DEVELOPMENT OF THE VELOCITY GRADIENT PROFILES WITH STREAMWISE DISTANCE

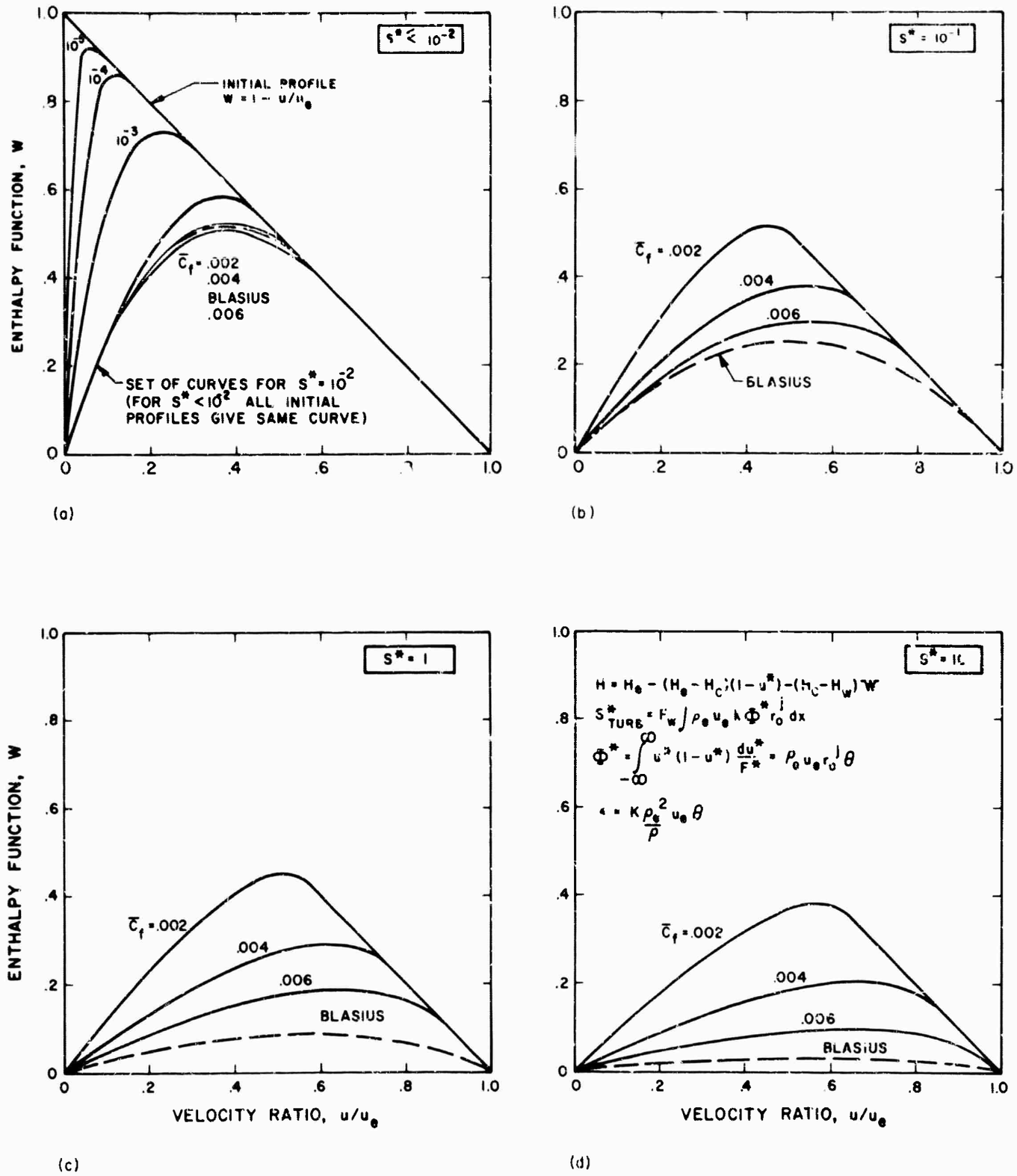

FIG. 11 DEVELOPMENT OF THE ENTHALPY FUNCTION W PROFILES WITH STREAMWISE DISTANCE

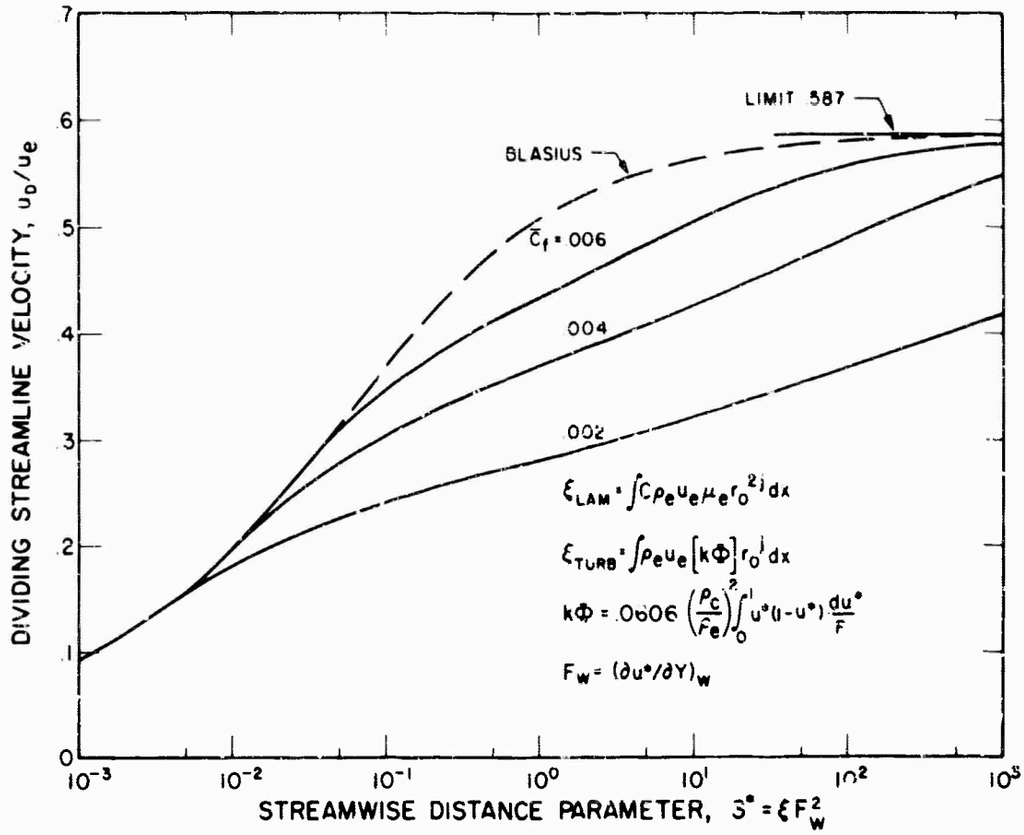

FIG. 12 VELOCITY ON THE DIVIDING STREAMLINE

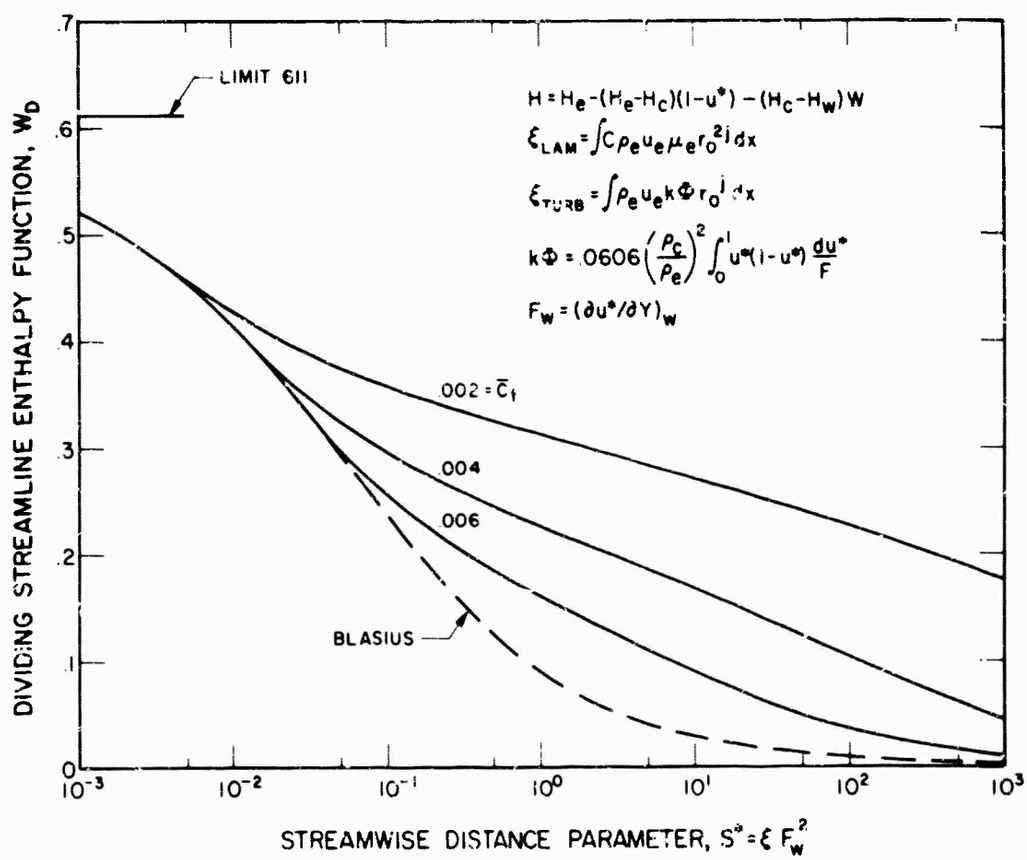

FIG. 13 ENTHALPY FUNCTION W ON THE DIVIDING STREAMLINE

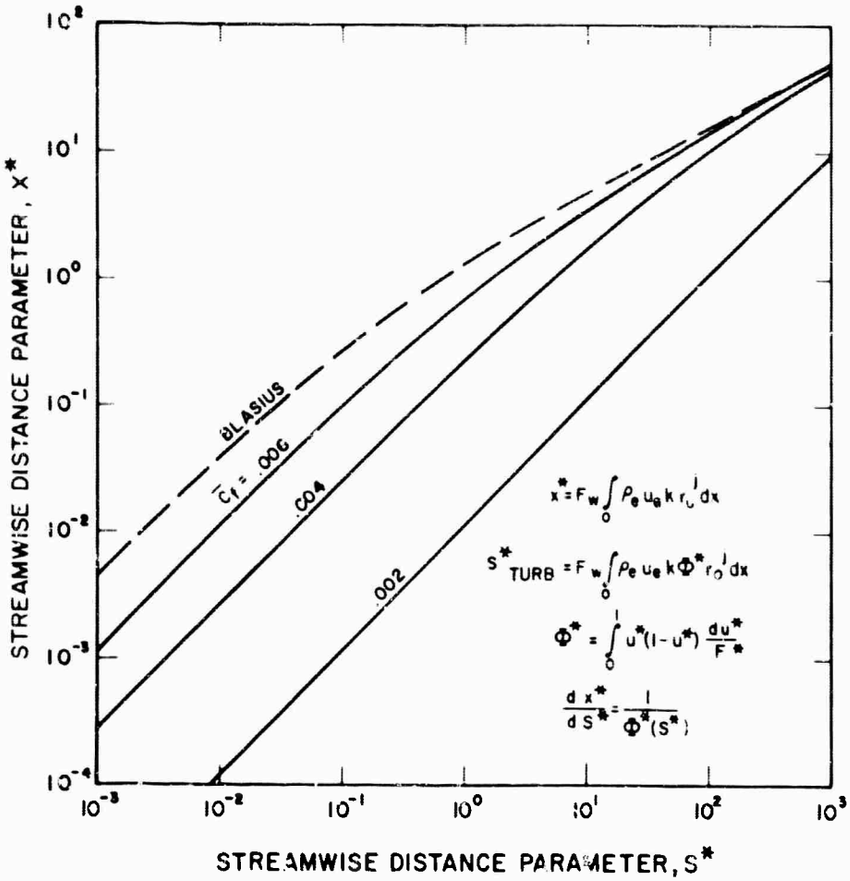

FIG. 14

RELATION BETWEEN x^* AND S^*

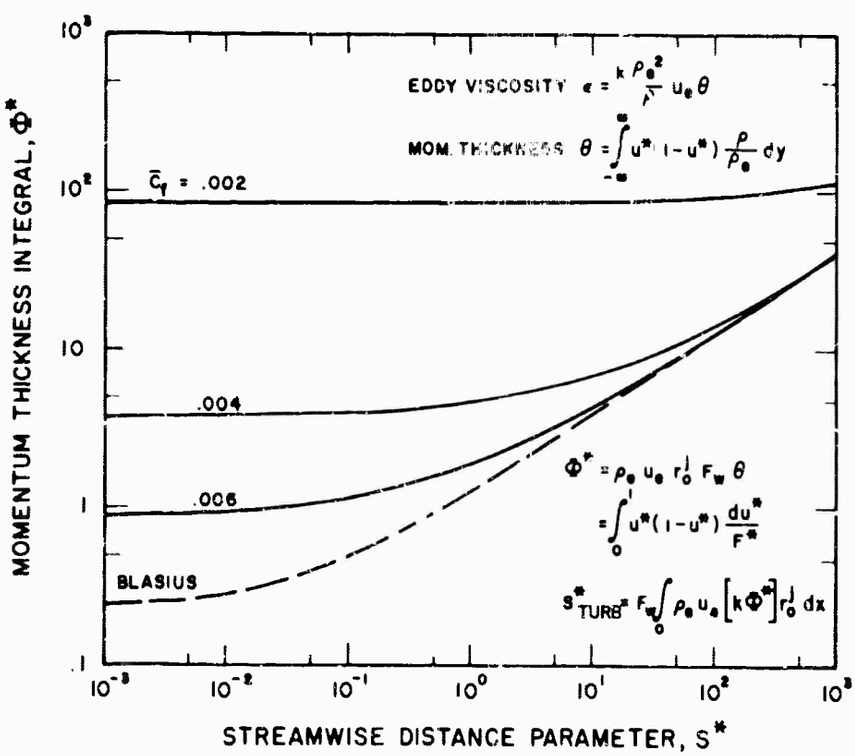

FIG. 15

SHEAR LAYER MOMENTUM THICKNESS INTEGRAL

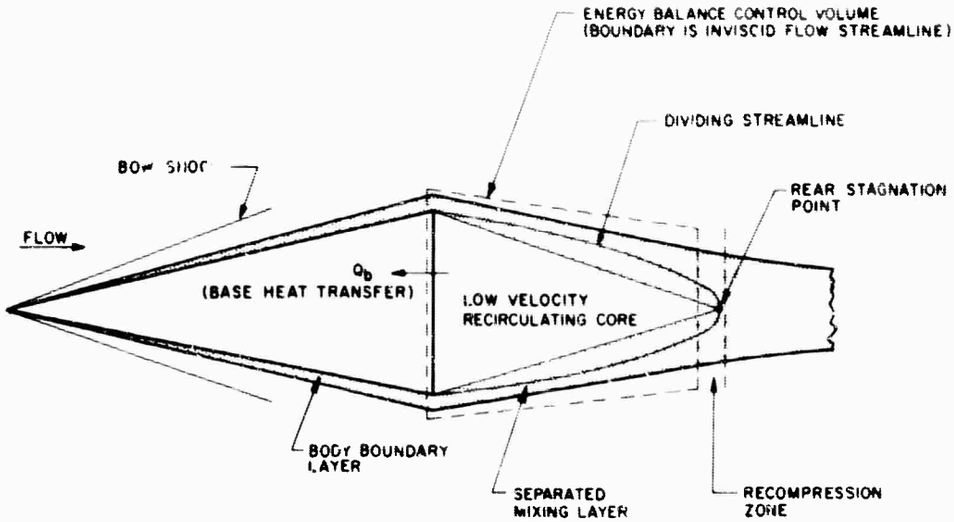

FIG. 16

BASE FLOW MODEL

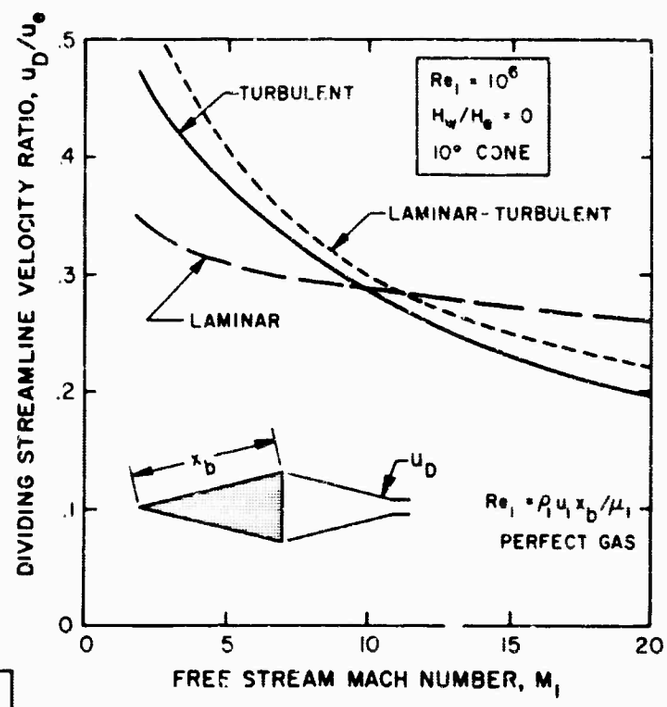

FIG. 17

DIVIDING STREAMLINE VELOCITY BEFORE RECOMPRESSION

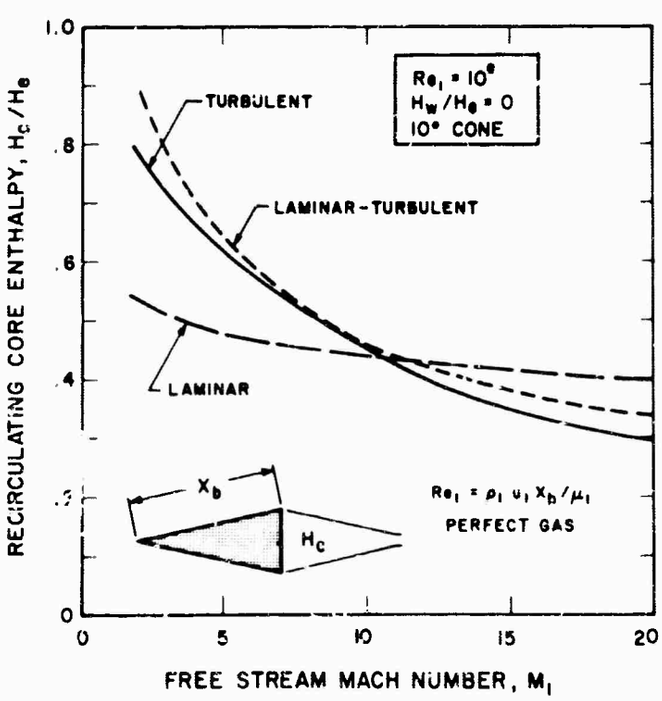

FIG. 18

RECIRCULATING REGION ENTHALPY

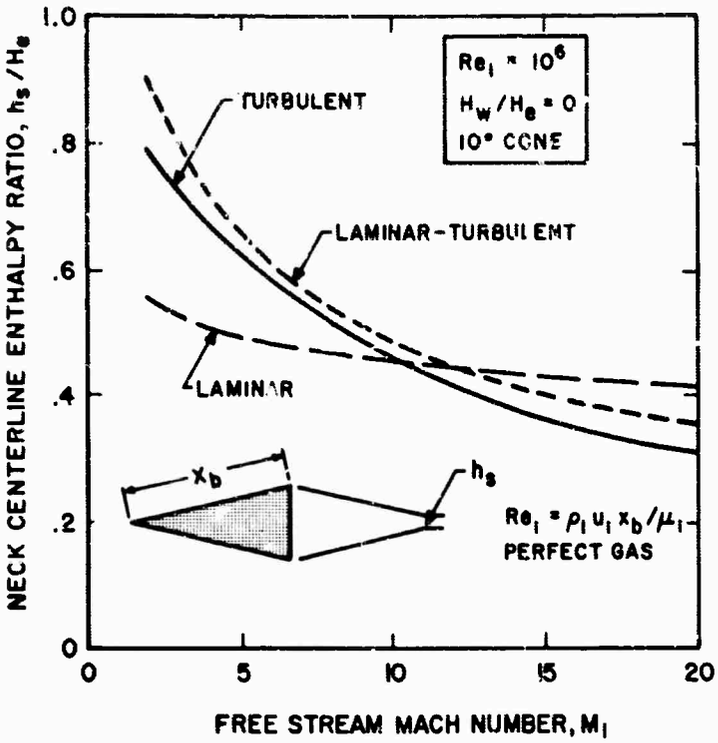

FIG. 19 EFFECT OF MACH NUMBER ON CENTERLINE STATIC ENTHALPY AFTER RECOMPRESSION

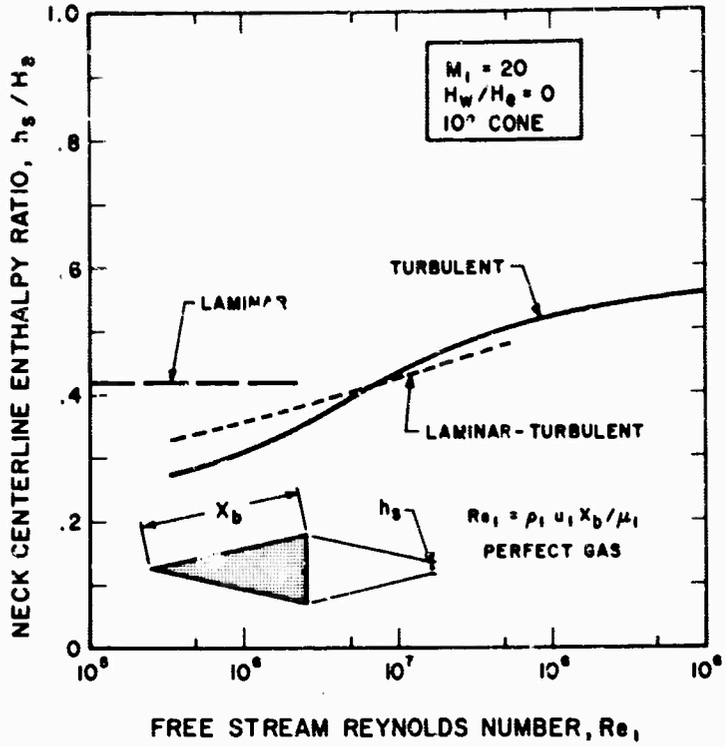

FIG. 20 EFFECT OF REYNOLDS NUMBER ON CENTERLINE STATIC ENTHALPY AFTER RECOMPRESSION

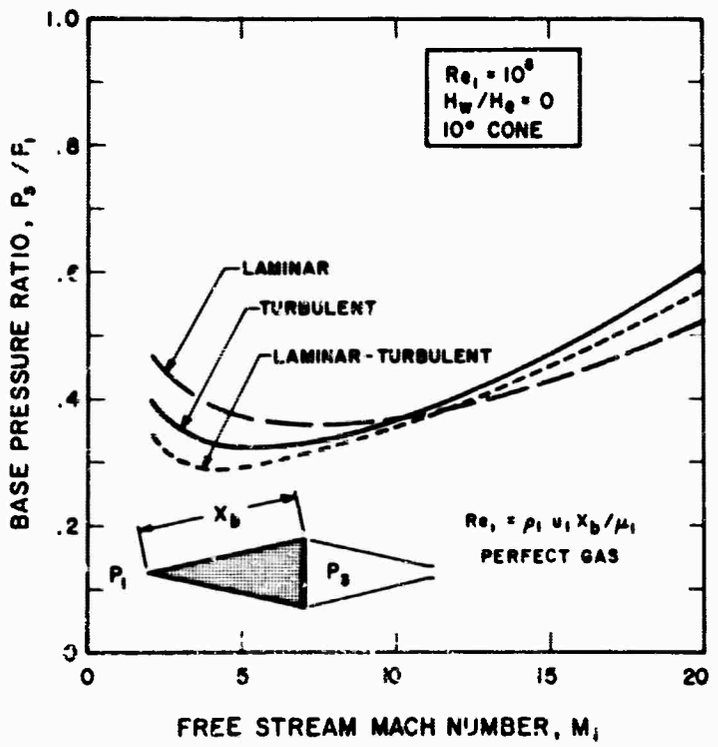

FIG. 21 EFFECT OF MACH NUMBER ON BASE PRESSURE

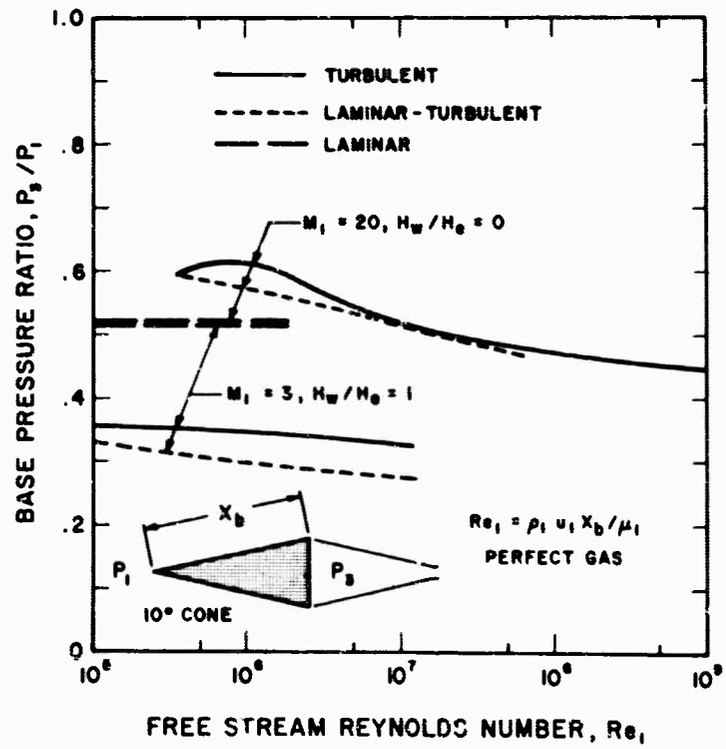

FIG. 22 EFFECT OF REYNOLDS NUMBER ON BASE PRESSURE